Atmos. Chem. Phys. Discuss., https://doi.org/10.5194/acp-2017-932
Manuscript under review for journal Atmos. Chem. Phys.
Discussion started: 10 November 2017

Atmospheric Chemistry and Physics
Open Access
EGU
Discussions

Direct radiative effects of intense Mediterranean desert dust outbreaks

Antonis Gkikas[1,2], Vincenzo Obiso[2], Carlos Pérez García-Pando[2], Oriol Jorba[2], Nikos Hatzianastassiou[3], Lluis Vendrell[2], Sara Basart[2], Santiago Gassó[4] and José Maria Baldasano[2,4]

[1]Institute for Astronomy, Astrophysics, Space Applications and Remote Sensing, National Observatory of Athens, Athens, 15236, Greece

[2]Earth Sciences Department, Barcelona Supercomputing Center, Barcelona, Spain

[3]Laboratory of Meteorology, Department of Physics, University of Ioannina, Ioannina, Greece

[4]Environmental Modelling Laboratory, Technical University of Catalonia, Barcelona, Spain

Corresponding author: Antonis Gkikas (agkikas@noa.gr)

Abstract

The direct radiative effect (DRE) of 20 intense and widespread dust outbreaks that affected the broader Mediterranean basin during the period March 2000 – February 2013, has been calculated with the regional NMMB-MONARCH model. The DREs have been calculated based on short-term simulations (84 hours) for a domain covering the Sahara and most part of the European continent. At midday, desert dust outbreaks induce locally a NET (shortwave plus longwave) strong atmospheric warming (DRE_{ATM} values up to 285 Wm^{-2}), a strong surface cooling ($DRE_{NETSURF}$ values down to -337 Wm^{-2}) whereas they strongly reduce the downward radiation at the ground (DRE_{SURF} values down to -589 Wm^{-2}). During nighttime, reverse effects of smaller magnitude are found. At the top of the atmosphere (TOA), positive (planetary warming) DREs up to 85 Wm^{-2} are found over highly reflective surfaces while negative (planetary cooling) DREs down to -184 Wm^{-2} are computed over dark surfaces at noon. Desert dust outbreaks significantly affect the regional radiation budget, with regional clear-sky NET DRE values ranging from -13.9 to 2.6 Wm^{-2}, from -43.6 to 4 Wm^{-2}, from -26.3 to 3.9 Wm^{-2} and from -3.7 to 28 Wm^{-2} for TOA, SURF, NETSURF and ATM, respectively. Although the shortwave (SW) DREs are larger than the longwave (LW) ones, the latter are comparable or even larger at TOA, particularly over the Sahara at midday. As a response to the strong surface cooling during daytime, dust outbreaks cause a reduction of the regional sensible and latent heat fluxes by up to 45 Wm^{-2} and 4 Wm^{-2}, respectively, averaged over land areas of the simulation domain. Dust outbreaks reduce the temperature at 2 meters by up to 4 K during day, whereas a reverse tendency of similar magnitude is found during night. Depending on the vertical distribution of dust loads and time, mineral particles heat (cool) the atmosphere

Atmos. Chem. Phys. Discuss., https://doi.org/10.5194/acp-2017-932
Manuscript under review for journal Atmos. Chem. Phys.
Discussion started: 10 November 2017

by up to 0.9 K (0.8 K) during daytime (nighttime) within atmospheric dust layers. Beneath and above the dust clouds, mineral particles cool (warm) the atmosphere by up to 1.3 K (1.2 K) at noon (night). When dust radiative effects are taken into account in numerical simulations, the total emitted dust and dust AOD, computed on a regional mean basis, are decreased (negative feedback) by 19.5% and 6.9%. The consideration of dust radiative effects in numerical simulations improves the model predictive skills. More specifically, it reduces the model positive and negative biases for the downward surface SW and LW radiation, respectively, with respect to Baseline Surface Radiation Network (BSRN) measurements. In addition, they also reduce the model near-surface (at 2 meters) nocturnal cold biases by up to 0.5 K (regional averages), as well as the model warm biases at 950 and 700 hPa, where the dust concentration is maximized, by up to 0.4 K.

1. Introduction

Dust aerosols through their interaction with the incoming solar (shortwave, SW) and the outgoing terrestrial (longwave, LW) radiation, perturb the radiation budget of the Earth-Atmosphere system and redistribute the energy therein. The induced perturbation of the radiation fields by dust particles, the so-called dust radiative effect, takes place through three processes of increasing complexity affecting the energy budgets at the surface, into the atmosphere and at the top of the atmosphere (TOA). The first one, known as direct radiative effect (DRE) and referred as REari (aerosol-radiation interactions) in the latest report of the Intergovernmental Panel on Climate Change (IPCC, Boucher et al., 2013), is caused by the absorption and scattering of the SW radiation (Sokolik et al., 2001) and the absorption and re-emission of the LW radiation by mineral particles (Heinold et al., 2008). Due to the perturbation of the radiation fields by dust aerosols, the energy budget both at the surface and into the atmosphere is modified and the signal of these impacts is evident in atmospheric stability/instability conditions associated with cloud development and precipitation. These rapid adjustments, which have been earlier referred as semi-direct effects (Hansen et al., 1997), are induced by the dust REari on surface energy budget and atmospheric profile (Boucher et al., 2013) contributing to the Effective Radiative Forcing (ERFari). Moreover, dust aerosols due to their ability to serve as cloud condensation nuclei (CCN) and ice nuclei (IN), modify the physical (Twomey, 1974; Albrecht, 1989) and optical properties of clouds (Pincus and Baker, 1994), which consist the major regulators of the Earth-Atmosphere system's radiation budget (Lohmann and Feicher, 2005). Through this chain of complex processes, it is described the indirect impact of mineral particles on the radiation and compared to the other two dust radiative effects (direct and semi-direct) is characterized by even larger uncertainties. In the latest IPCC report (IPCC, 2013), the formerly known

Atmos. Chem. Phys. Discuss., https://doi.org/10.5194/acp-2017-932
Manuscript under review for journal Atmos. Chem. Phys.
Discussion started: 10 November 2017

Atmospheric Chemistry and Physics
Discussions

as indirect effects have been renamed to Effective Radiative Forcing (ERFaci) including the modification of radiation by clouds, attributed to aerosol-cloud interactions (aci), as well as the subsequent changes (rapid adjustments) of clouds' physical/microphysical/optical properties (Boucher et al., 2013).

Several studies have been conducted aiming at estimating the dust direct/semi-direct (e.g. Pérez et al., 2006; Helmert et al., 2007; Zhao et al., 2010; Nabat et al., 2015a) and indirect effects (e.g. Sassen et al., 2003; Seigel et al., 2013). Specifically, numerous studies have been carried out either by means of numerical modelling (e.g. Solmon et al., 2012; Woodage and Woodward, 2014) or through the synergy of observations and radiative transfer codes (Di Sarra et al., 2011; Valenzuela et al., 2012) or solely based on aerosol observations (e.g. Yang et al., 2009; Zhang et al., 2016) and their findings either referred to extended (e.g. Spyrou et al., 2013) or limited time periods (e.g. Nabat et al., 2015b) or to specific desert dust outbreaks (e.g. Pérez et al., 2006; Santese et al., 2010; Stanelle et al., 2010). The investigation of dust radiative effects is a scientific issue of great concern since it is documented that mineral particles, through their interaction with the radiation, can affect atmospheric processes from short (weather) to long (climate) temporal scales. To this aim, many research efforts were dedicated to the investigation of dust impacts on the convective activity (Mallet et al., 2009), sea surface temperature (Foltz and McPhaden, 2008), hydrological cycle (Miller et al., 2004b), hurricanes (Bretl et al., 2015), boundary layer dynamics (Heinold et al., 2008) and monsoons (Solmon et al., 2008; Vinoj et al., 2014).

The direct impact of dust aerosols is expressed by the sign and the magnitude of the DRE values, which are defined as the anomalies (perturbation) of the radiation attributed to dust-radiation direct interaction, considering as a reference (control) an atmospheric state where mineral particles are not a radiatively active substance. Based on this, negative and positive DREs indicate a cooling (loss of energy) and a warming effect (gain of energy), respectively. Nevertheless, the sign of the DREs varies between the SW and LW spectrum (Osborne et al., 2011) as well as within the Earth-Atmosphere system. More specifically, due to the attenuation (through scattering and absorption) of the SW radiation, dust aerosols warm the atmosphere and cool the surface (Huang et al., 2014), while reverse tendencies are revealed at longer wavelengths attributed to the absorption and re-emission of LW radiation by the mineral particles (Sicard et al., 2014a). Between the two spectrum ranges, the SW DREs are larger compared to the LW ones, in absolute terms, explaining thus their predominance when the corresponding calculations are made for the NET (SW+LW) radiation (e.g. Pérez et al., 2006; Zhu et al., 2007; Woodage et al., 2014). The perturbations of the radiation budget at the surface and into the atmosphere determine the DRE at TOA (e.g. Kumar et al., 2014), which indicates the increase (planetary cooling) or the decrease (planetary warming) of the outgoing radiation from the Earth-Atmosphere system and is relevant to dust climatic effects (Christopher and Jones, 2007).

The scientific importance of investigating the dust direct impacts on radiation has been notified in previous studies where it was shown that the consideration of the dust-radiation interactions may improve the forecasting ability of weather models (Pérez et al., 2006) and can reduce the observed biases of the LW radiation at TOA between models and satellite retrievals (Haywood et al., 2005). The dust direct impacts are highly variable both in space (e.g. Zhao et al., 2010) and time (e.g. Osipov et al., 2015) attributed to several parameters related either to dust aerosols' physical and optical properties or to external factors (e.g. surface type), which determine both the sign and the magnitude of the DREs (Liao and Seinfeld, 1998). One of the most important factor is the composition of mineral particles determining the spectral variation of the refractive index (Müller et al., 2009; Petzold et al., 2009) and subsequently their absorption efficiency (Mallet et al., 2009), which are both critical in radiation transfer studies, and are also dependent on the mixing state (either external or internal) of dust aerosols (Scarnato et al., 2015). Under clear skies, apart from mineral particles' optical properties, the shape (Wang et al., 2013a), the emitted dust size distribution (Mahowald et al., 2014), the surface albedo (Tegen et al., 2010) as well as the vertical distribution of dust aerosols (Mishra et al., 2015) have been recognized as determinant factors for the DRE calculation. On the contrary, when clouds are present, the position of dust layers with regards to clouds defines the sign and the magnitude of DREs at TOA (Yorks et al., 2009; Meyer et al., 2013; Choobari et al., 2014; Zhang et al., 2014).

The dust radiative effects become important under specific conditions of very high concentrations, so-called events or episodes or outbreaks. Such episodes occur frequently over the broader Mediterranean basin (Gkikas et al., 2013), due to its vicinity to the world's major dust sources situated across the northern Africa (Sahara) and Middle East deserts (Ginoux et al., 2012). Dust particles are mobilized over these areas by strong winds (Schepanski et al., 2009) being uplifted to the free troposphere due to strong convection in the boundary layer (Cuesta et al., 2009) and are transported towards the Mediterranean due to the prevailing atmospheric (synoptic) circulation (Gkikas et al., 2015). Under these conditions, dust particles over the Mediterranean are recorded at very high concentrations as it has been confirmed either by satellite (e.g. Moulin et al., 1998; Guerrero-Rascado et al., 2009; Rémy et al., 2015) and ground retrievals (e.g. Kubilay et al., 2003; Toledano et al., 2007) or by surface PM_{10} measurements (e.g. Rodríguez et al., 2001; Querol et al., 2009; Pey et al., 2013).

Among the different aerosol types that co-exist in the Mediterranean (Lelieveld et al., 2002; Basart et al., 2009), dust is the one causing the greatest perturbation of the SW and LW radiation, especially during desert dust outbreaks (e.g. Di Sarra et al., 2008; Di Biagio et al., 2010). Thus, a number of studies focused on Mediterranean dust outbreaks' impacts on the SW (Meloni et al., 2004; Gómez-Amo et al., 2011; Antón et al., 2012; Di Sarra et al., 2013; Obregón et al., 2015), LW (Antón et al., 2014; Sicard et al., 2014a) and NET (Di Sarra et al., 2011; Romano et al., 2016) radiation. However, the obtained results were representative at a local scale and considering the high spatial variability of desert dust outbreaks, the optimum solution of assessing in a comprehensive way their impacts on weather and climate is provided by atmospheric-dust models. To this aim, the induced DREs by the Mediterranean desert dust outbreaks have been analyzed through short-term numerical simulations (Pérez et al., 2006; Santese et al., 2010; Remy et al., 2015), revealing strong perturbations of the energy budget within the Earth-Atmosphere system, which in turn affect atmospheric processes. Moreover, similar studies have been conducted either at a seasonal (Nabat et al., 2015a) and annual scale (Nabat et al., 2012) or for extended time periods (Spyrou et al., 2013; Nabat et al., 2015b) pointing out the key role of desert dust aerosols in the Mediterranean climate.

The overarching goals of the present study are: (i) the assessment of the short-term direct radiative effects (DREs) on the Earth-Atmosphere system's radiation budget, induced by intense Mediterranean desert dust outbreaks, based on regional model simulations, (ii) the assessment of the associated impacts on temperature and sensible/latent heat fluxes, (iii) the investigation of possible feedbacks on dust AOD and dust emission and (iv) the assessment of the model's predictive skills, in terms of reproducing temperature and radiation fields, when dust-radiation interactions are taken into account in numerical simulations. To this aim, 20 intense and widespread desert dust outbreaks that affected the broader area of the Mediterranean basin, over the period March 2000 – February 2013, have been identified based on an objective and dynamic satellite algorithm (Section 2). It must be highlighted that through the consideration of a large dataset of desert dust outbreaks is ensured the robustness of our findings, providing thus the opportunity to have a clear view of dust outbreaks' impacts on radiation as well as about the associated impacts on meteorological variables (e.g. temperature). For each dust outbreak, through short-term (84 h) numerical simulations of the regional NMMB-MONARCH model (Section 3), the DREs are calculated at TOA, surface and into the atmosphere, both at grid point (geographical distributions) and regional scale level (Section 5.2), for the SW, LW and NET (SW+LW) radiation. In addition, are examined the impacts of the Mediterranean desert dust outbreaks on the sensible/latent heat fluxes (Section 5.3) and on the surface temperature (Section 5.4) as well as the potential feedbacks on dust AOD and dust emissions (Section 5.5). The last part of the study (Sections 5.6 and 5.7) investigates the potential improvement of the model's forecasting ability in terms of reproducing the temperature and radiation fields when dust-radiation interactions are included in numerical simulations. A summary is made and conclusions are drawn in Section 6.

2. Selection of desert dust outbreaks

In the present study, 20 intense and widespread desert dust outbreaks that affected the broader area of the Mediterranean basin, over the period March 2000 – February 2013, are analyzed. The studied desert dust outbreaks have been identified using an objective and dynamic satellite algorithm introduced in Gkikas et al. (2013) and further developed in Gkikas et al. (2016). The algorithm utilizes daily 1° x 1° latitude-longitude resolution satellite retrievals, derived from MODerate resolution Imaging Spectroradiometer (MODIS; Remer et al., 2005), Total Ozone Mapping Spectrometer (TOMS; Torres et al., 1998) and Ozone Monitoring Instrument (OMI; Torres et al., 2007) observations. The MODIS-Terra (Collection 051) aerosol optical depth at 550nm (AOD_{550nm}), Ångström exponent (α), fine fraction (FF) and effective radius (r_{eff}, available only over sea) products are used in the algorithm along with EP-TOMS and OMI-Aura Aerosol Index (AI). Using these products, the algorithm takes into account information regarding aerosols' load (AOD), size (FF, a and r_{eff}) and absorbing/scattering ability (AI) which is necessary for the identification of dust.

Only a brief discussion of the algorithm operation is given here, whereas a detailed description is provided in Gkikas et al. (2013). The satellite algorithm is applied to each individual 1° x 1° grid cell of the Mediterranean Satellite Domain (29° N - 47° N and 11° W - 39° E, MSD, red rectangular in Figure 1) during the period March 2000 – February 2013. For each grid cell, from the series (2000-2013) of daily AOD_{550nm} values, the mean ($Mean$) and the associated standard deviation (Std) of AOD_{550nm} are calculated. Based on these two primary statistics, two threshold (or cut-off) levels being equal to $Mean+2*Std$ and $Mean+4*Std$, are defined. By comparing each daily AOD value to the two thresholds, the algorithm determines whether an aerosol episode (or event) occurs over an 1° x 1° grid cell in that day or not, and labels it as strong or extreme, depending on which AOD threshold is exceeded (lower or higher). Thereby, the term "aerosol episode" refers to pixel-level episodic (extremely high loading) aerosol conditions and it is used with this meaning henceforth. Subsequently, in order to characterize the identified pixel-level episodes as desert dust (DD) ones, appropriate thresholds for α, FF, r_{eff} and AI are used, based on existing knowledge about relevant physical properties (size and absorbing/scattering ability) of dust. According to the algorithm, a strong or extreme pixel-level DD episode occurs if $\alpha \leq 0.7$, $FF \leq 0.4$, $r_{eff} > 0.6$ μm and $AI > 1$ (conditions should be met simultaneously).

Based on the satellite algorithm's outputs, for each day of the study period it is calculated the total number of grid cells over which a strong or an extreme DD episode has taken place. Subsequently, from the overall series of 4748 days over the study period, are kept only those in which at least 30 grid cells with a DD episode (either strong or extreme) have been recorded. This criterion was first adopted by Gkikas et al. (2015), who analyzed the atmospheric circulation evolution patterns favoring the occurrence of dust outbreaks over the broader Mediterranean basin, in order to keep and study the most extensive ones (in terms of the number of pixel-level DD episodes). In a next step, the days satisfying the defined criterion (i.e. days where at least 30 pixel-level DD episodes have been occurred) are ranked based on their regional MODIS-Terra AODs averaged over the "dust episodic" pixels within the geographical limits of the MSD. If two or more consecutive days are satisfying the defined criteria, then the day with the maximum number of DD episodes is selected. The final dataset consists of 20 intense Mediterranean desert dust outbreaks listed in a chronological order in Table 1.

The majority of the selected desert dust outbreaks (55 % or 11 out of 20) took place in spring (March-April-May) when massive dust loads originating in the Sahara Desert are transported towards the central and eastern parts of the Mediterranean (Gkikas et al., 2013; Pey et al., 2013). Four widespread desert dust outbreaks affected mainly the western sector of the MSD in summer (July, August), while five dust outbreaks were recorded across the central and eastern parts of the basin in winter (January, February). Among the selected cases, the number of pixel-level DD episodes in the MSD varies from 30 (28 July 2005, western-central Mediterranean) to 85 (31 July 2001, western Mediterranean), whereas their intensity (in terms of AOD at 550nm) ranges from 0.74 (31 July 2001) to 2.96 (2 March 2005), being in general higher in winter while moderate-to-high intensities are recorded in spring. Based on the information in Table 1, the selected study cases correspond to widespread and intense dust outbreaks that occurred in various parts of the Mediterranean, and therefore they are representative and appropriate for further studying their radiative effects. The occurrence of intense desert dust outbreaks during the first half of the year is favored either by the predominance of intense low pressure systems across the Mediterranean basin (Varga et al., 2014; Gkikas et al., 2015) or by their eastwards shift (Saharan depressions) across the northern coasts of Africa (Alpert and Ziv, 1989). In both seasons, dust transport from the northern Africa deserts towards the Mediterranean is induced by the prevailing southerly or southwesterly airflow (Barkan et al., 2005; Meloni et al., 2008). Some of the identified desert dust outbreaks here, have been also analyzed in previous studies related to particulate matter levels (Kanakidou et al., 2010), chemical speciation (Theodosi et al., 2010), dust layers' vertical structure (Amiridis et al., 2009; DeSouza-Machado et al., 2010), dust radiative effects (Di Sarra et al., 2011), dust modelling (Carnevale et al., 2012) and prevailing synoptic conditions favoring the occurrence of dust events (Nastos, 2012).

3. Model description

In the present section, the main features of the meteorological driver (Section 3.1.1) and the dust module (Section 3.1.2) used in the regional NMMB-MONARCH (Multiscale Online Nonhydrostatic AtmospheRe CHemistry) model, previously known as NMMB/BSC-Dust, are described. The version (v1.0) of the NMMB-MONARCH model used here contributes to different model inter-comparisons like the International Cooperative for Aerosol Prediction (ICAP) initiative and the Sand and Dust Storm Warning Advisory and Assessment System (SDS-WAS), a project developed under the umbrella of the World Meteorological Organization (WMO) with focus on improving capabilities of sand and dust storm forecasts. For brevity reasons, only the main characteristics of the model are discussed here since a thorough description is provided in Pérez et al. (2011, and references therein) as well as in recent publications presenting its developments and applications in gas-phase chemistry (Badia et al., 2017), volcanic ash dispersion (Marti et al., 2017) and data assimilation (Di Tomaso et al., 2017) studies. The spectral variation of the GOCART dust optical properties, utilized as inputs to the radiation transfer scheme, is presented in Section 3.2, whereas the model set up used in our experiments is given in Section 3.3.

3.1. The NMMB-MONARCH model

3.1.1. The NMMB atmospheric model

The Non-hydrostatic Multiscale Model NMMB (Janjic, 2004; Janjic and Black, 2007; Janjic et al., 2011) is a unified atmospheric model developed at the National Centers for Environmental Prediction (NCEP) (Janjic et al., 2001; Janjic, 2003). A powerful element of the model constitutes its non-hydrostatic dynamical core, activated depending on the resolution, providing the capability to be used for applications spanning at a wide range of temporal (from short- to long-term) and spatial (from regional to global) scales. An additional dynamic feature of the NMMB is the consideration of various parameterization schemes which can be incorporated into the numerical simulations. In our simulations, the parameterization schemes of Betts-Miller-Janjic (Betts, 1986; Betts and Miller, 1986; Janjic, 1994, 2000), Ferrier (Ferrier et al., 2002), Mellor-Yamada-Janjic (Janjic et al., 2001) and Monin-Obukhov (Monin and Obukhov, 1954) have been utilized for the convection, cloud microphysics, turbulence and surface layer, respectively, as well as the NOAH land model (Ek et al., 2003). The model's dynamic equations, in the horizontal plane, are solved on the Arakawa B grid (Arakawa and Lamb, 1977) while in vertical the general hybrid pressure-sigma coordinate (Simmons and Burridge, 1981) is utilized. For regional simulations, a rotated longitude-latitude coordinated system is used (the Equator is running through the middle of the integration domain) enabling therefore more uniform grid distances.

3.1.2. The Dust component

The main components of the desert dust life cycle, regarding mineral particles' production in the source areas, transport and removal from atmosphere, are considered in the dust component of the MONARCH model, which is embedded into the NMMB model. The size intervals as well as the effective radii for each one of the 8 dust bins, representing clay-originated sub-micron (bins 1-4) and silt-originated coarse (bins 5-8) particles, that are considered in the dust module were adopted from Pérez et al. (2006). The mass of each bin is calculated at each time step, grid point and layer, while the median mass diameter and the geometric standard deviation of the sub-bin distribution are fixed to 2.524 μm and 2.0 μm, respectively. All the required parameters regulating dust emission and mobilization namely the: (i) surface wind speed, (ii) turbulence, (iii) land use type, (iv) vegetation cover, (v) erodibility, (vi) surface roughness, (vii) soil texture and (viii) soil moisture, are considered in the dust emission scheme (Pérez et al., 2011). The vertical dust flux for each dust size bin is proportional to the horizontal sand flux while several parameters are tuned to match observations that are mainly available far away from the sources. Coarse dust aerosols are removed efficiently from the atmosphere through sedimentation, which is solved implicitly in each model layer. For the description of dust aerosols' wet removal, a mechanism which is more effective for fine mineral particles, parameterizations representing in- and below-cloud scavenging are included in the NMMB-MONARCH in which the grid-scale cloud microphysical scheme of Ferrier and the convective adjustment scheme of Betts-Miller-Janjic are utilized (Pérez et al., 2011). The ability of the NMMB-MONARCH model to reproduce accurately the dust aerosol fields has been confirmed through evaluation studies, relied on annual simulations, both at regional and global (Pérez et al., 2011) scale as well as by utilizing measurements from experimental campaigns as reference data (Haustein et al., 2012). Moreover, the reliability of the model in terms of reproducing the Saharan dust patterns over Cape Verde as well as to simulate dust vertical profiles have been confirmed through the analyses made by Gama et al. (2015) and Binietoglou et al. (2015), respectively. Finally, the predictive skills of the NMMB-MONARCH model, in comparison with other regional models, have been assessed for a specific dust outbreak (Huneeus et al., 2016) that affected the western parts of the Mediterranean and Europe.

Atmos. Chem. Phys. Discuss., https://doi.org/10.5194/acp-2017-932
Manuscript under review for journal Atmos. Chem. Phys.
Discussion started: 10 November 2017

3.2. Radiation transfer scheme and dust optical properties

For the description of dust aerosols interaction both with the shortwave (SW) and longwave (LW) radiation, the RRTMG (Rapid Radiative Transfer Model, Mlawer et al., 1997; Iacono et al., 2008) radiation transfer scheme is coupled with the dust module. RRTMG consists a modified version of the RRTM which is a broadband radiative transfer model that includes the molecular absorption of the SW (by water vapor, carbon dioxide, ozone, methane and oxygen) and LW (by water vapor, carbon dioxide, ozone, methane, nitrous oxide, oxygen, nitrogen and halocarbons) radiation. Even though the basic physics and absorption coefficients utilized in RRTM remain unchanged in RRTMG, several updates regarding computational efficiency and representation of subgrid-scale cloud variability have been considered (Iacono et al., 2008). Through these adjustments, it has been improved the efficiency of the RRTMG in global circulation model (GCM) applications with a minimal loss of accuracy (Iacono et al., 2008). In the RRTMG, the total number of quadratic points (g points) used to calculate radiances has been reduced from 224 to 112 and from 256 to 140 for the shortwave and longwave spectrum, respectively. In addition, for the short wavelengths, the discrete ordinates algorithm DISORT (Stammes et al., 1998) has been replaced by a two-stream radiation transfer solver (Oreopoulos and Baker, 1999). All the updates applied in the RRTMG radiation transfer code are listed in the Atmospheric and Environmental Research (AER) radiative transfer web site (http://www.rtweb.aer.com). Based on evaluation studies, the comparison of the RRTMG clear-sky SW and LW fluxes versus RRTM_SW and LBLRTM, respectively, has revealed that its accuracy at short wavelengths is within 3 Wm^{-2} whereas at long wavelengths is 1.5 Wm^{-2}. As inputs to the radiation transfer scheme, the aerosol optical depth (AOD, measure of the aerosol load), the single scattering albedo (SSA, expresses the percentage of scattering to total extinction) and the asymmetry parameter (ASYM, expresses the angular distribution of the scattered radiation) are required. In the present version (v1.0) of the model, the calculation of dust optical properties is made based on the formulas presented in Pérez et al. (2006), by using the mass concentration simulated by the NMMB-MONARCH model and the single-particle optical properties derived by the GOCART model (Chin et al., 2002). The spectral variation of the single-particle optical properties for each bin, namely the mass extinction coefficient, the single scattering albedo and the asymmetry parameter are shown in Figures 2-i, 2-ii and 2-iii, respectively. Their calculation for each dust size bin and at each spectral band is made based on the Mie code (Mishchenko et al., 2002) assuming homogeneous and spherical dust particles. For the other types of tropospheric aerosols (sulfate, organic carbon, black carbon, and sea salt), the GOCART monthly climatological AOD, SSA and ASYM values

Atmos. Chem. Phys. Discuss., https://doi.org/10.5194/acp-2017-932
Manuscript under review for journal Atmos. Chem. Phys.
Discussion started: 10 November 2017

are utilized.

3.3. Model set-up configuration

In our experiments, the simulation domain (NMMB-MONARCH Simulation Domain, NSD, outer domain in Figure 1) covers the Sahara (dust sources areas), the Mediterranean (mid-range dust transport areas) as well as most of the European continent (long-range dust transport areas). The horizontal resolution is equal to 0.25° x 0.25° degrees and 40 sigma-hybrid pressure levels up to 50 hPa are used in vertical. The atmospheric model's fundamental time step is set to 25 seconds. The simulations have been made for each one of the 20 identified Mediterranean desert dust outbreaks (see Section 2) considering a spin-up and a forecast period, using 1° x 1° NCEP final analyses (FNL) as initial and 6-h boundary conditions. More specifically, for each case, a hindcast period of 84 hours starts at 00 UTC of the day (see the second column in Table 1) when the desert dust outbreak has been identified according to the defined criteria (explained in Section 2). In order to ensure a more "realistic" initial state of the atmosphere, a 10-day spin-up before the initialization of the forecast period is simulated, where the model's meteorology is reinitialized every 24 hours. For the forecast periods, for the computation of the dust radiative effects, two configurations of the model were run. In the first one (RADON), aerosols interact with the short- and longwave radiation while in the second one the corresponding interactions are deactivated (RADOFF).

4. Calculation of the dust direct radiative effects

The direct radiative effects (DREs), expressed in Wm^{-2}, are computed at the top of the atmosphere (TOA), into the atmosphere (ATM), and at the surface, for the downwelling (SURF) and the absorbed (NETSURF) radiation, for the shortwave (SW), longwave (LW) and NET (SW+LW) radiation. The calculations are made according to the following formulas:

$DRE_{TOA} = F^{\uparrow}_{TOA,RADOFF} - F^{\uparrow}_{TOA,RADON}$ (Eq. 1)

$DRE_{SURF} = F^{\downarrow}_{SURF,RADON} - F^{\downarrow}_{SURF,RADOFF}$ (Eq. 2)

$DRE_{NETSURF} = \left(F^{\downarrow}_{SURF,RADON} - F^{\uparrow}_{SURF,RADON}\right) - \left(F^{\downarrow}_{SURF,RADOFF} - F^{\uparrow}_{SURF,RADOFF}\right) = F_{NETSURF,RADON} - F_{NETSURF,RADOFF}$ (Eq. 3)

$DRE_{ATM} = DRE_{TOA} - DRE_{NETSURF}$ (Eq. 4)

At TOA (Eq.1), DREs are calculated through the subtraction of the RADON (dust-radiation interaction is activated) from the RADOFF (dust-radiation interaction is deactivated) outputs of the upward (↑) radiative fluxes (F) and express the loss (cooling effect or planetary cooling) or the gain (warming effect or planetary warming) of energy within the Earth-Atmosphere system when are negative and positive, respectively. At the surface, DREs are computed for both the downwelling (↓) (SURF, Eq. 2) and the net (downward minus upward) radiation (NETSURF, Eq. 3). Both DREs indicate a dust-induced surface cooling or warming when they get negative or positive values, respectively. Finally, on energy within the Earth-Atmosphere system, the DRE_{ATM} is calculated by subtracting the $DRE_{NETSURF}$ from the DRE_{TOA} values (Eq. 4) and quantifies the impact (warming or cooling) of dust outbreaks on the atmospheric radiation budget. The DREs are based on the subtraction of two independent model runs. Therefore, our results represent the radiative anomalies by dust aerosols including both the direct effect and the fast response of atmospheric constituents such as humidity and clouds (semi-direct effects). DREs are analyzed both at grid point (geographical distributions) and at regional scale levels and the obtained results will be discussed in Section 5.2.

5. Results

5.1. Comparison of model and satellite AODs

Before dealing with the DREs, the ability of the model to reproduce satisfactorily the dust AOD fields is assessed using MODIS-Terra AOD_{550nm} retrievals as reference data. The results of the intercomparison between the daily satellite AODs (left column in Fig. 3) and the modelled (right column in Fig. 3) dust AODs at 12 UTC are presented here for three of the 20 identified desert dust outbreaks (see Section 2), which took place on 2nd March 2005 (upper row in Fig. 3), 19th May 2008 (middle row in Fig. 3) and 2nd August 2012 (bottom row in Fig. 3) and affected the eastern, central and western parts of the Mediterranean basin, respectively. The corresponding maps for the remaining 17 cases are illustrated in Figure S1. Note, that the evaluation of the model outputs versus the satellite measurements is restricted within the geographical limits of the MSD (red rectangle in Fig. 1), since the satellite algorithm used for identification of the desert dust outbreaks is applied only to this region (see Section 2).

According to the MODIS-Terra observations on 2nd March 2005, a dust plume extends from the Gulf of Sidra to the southern parts of Greece, with AODs up to 5 (Fig. 3 i-a). As shown in Fig. 3 i-b, the model

Atmos. Chem. Phys. Discuss., https://doi.org/10.5194/acp-2017-932
Manuscript under review for journal Atmos. Chem. Phys.
Discussion started: 10 November 2017

is able to reproduce satisfactorily the spatial patterns of AOD on this day, with high dust AOD_{550nm} values (1-4) extending from Algeria to the Black Sea, affecting the eastern parts of the Mediterranean Sea. There is a good agreement between the model and the satellite over areas where the satellite measurements are available, highlighting the ability of the model to capture satisfactorily the spatial features of dust loads. Nevertheless, several factors affect the level of agreement between model outputs and satellite observations and for this reason only a qualitative intercomparison is attempted. The most important of them are related to the differences regarding the spatiotemporal resolution and the aerosol optical depth product. MODIS provides daily total AODs at 1° x 1° spatial resolution in contrast to the NMMB-MONARCH model which produces instantaneous dust AODs at 0.25° x 0.25° spatial resolution. Moreover, due to the inability of the MODIS Dark Target (DT) algorithm to retrieve aerosol optical properties over desert areas as well as under cloudy conditions, in a significant part of the study region there are not available satellite observations (white areas in Figs. 3 i-a, ii-a and iii-a) restricting thus their comparison with the model outputs which provide full spatial coverage.

The second desert dust outbreak occurred on 19th May 2008 and affected the central sector of the MSD. According to MODIS (Fig. 3 ii-a), the intensity of dust loads is maximized (up to 4) in the central parts of the Mediterranean Sea (southeastern of Sicily). This is also reproduced by the model, although somewhat higher AODs are found over the central and southern parts of Italy (Fig. 3 ii-b). In spite of this, however, there is a clearly good model performance in reproducing the dust event that hit the central Mediterranean. An ever better agreement between the model and satellite AODs, in terms of spatial variability and intensity of dust loads, is found for the desert dust outbreak of August 2nd 2012, that affected the westernmost parts of the Mediterranean, with highest AODs (up to 2-2.5) from the Alboran Sea down to the coastal areas of Morocco (Figs. 3 iii-a,b). The model's ability to reproduce correctly the spatial patterns and values of dust AODs is crucial for a successful computation of the dust DREs, since DREs are determined to a large extent by AOD (e.g. Hatzianastassiou et al., 2004; Pérez et al., 2006; Papadimas et al., 2012).

5.2. Direct radiative effects (DREs)

5.2.1. Geographical distributions

For each desert dust outbreak, the TOA, ATM, SURF and NETSURF DREs have been computed for the SW, LW and NET radiation, according to the formulas presented in Section 4. Just as an example, in Figure 4 are illustrated the geographical patterns of the instantaneous NET (SW+LW) DRE_{TOA} (second column), DRE_{ATM} (third column), DRE_{SURF} (fourth column) and $DRE_{NETSURF}$ (fifth column) values, at

12 h (first row), 24 h (second row), 36 h (third row) and 48 h (fourth row) after the initialization of the model forecast on 2nd August 2012 at 00 UTC, along with the simulated patterns of dust AOD at 550 nm on the same day and time (first column). For brevity reasons only the results for the all wave (NET) are given, while the SW and LW DREs and their contribution to NET DREs are discussed in the regional analysis (next sub-section). Moreover, for each desert dust outbreak, the minimum and maximum clear-sky NET DREs at grid point level, during the simulation period, are presented in Table S1.

Based on the model outputs, at 12 h, an arc shaped dust plume affected the western parts of the Sahara, the Canary Islands, the maritime areas off the Moroccan coasts, the southern parts of the Iberian Peninsula and the western Mediterranean Sea (Fig. 4). During the forecast period, the spatial features of the desert dust outbreak do not reveal a remarkable variability, with maximum AODs (up to 3) across Mali, Mauritania, Western Sahara and in the Canary Islands. According to the simulated atmospheric circulation patterns (results not shown here), strong near surface winds prevail across a convergence zone (in western Sahara) developed between a low pressure system with its center in Mauritania-Mali and the Azores subtropical anticyclone. At 700 hPa (~ 3000 meters), the uplifted mineral particles are transported towards the western Mediterranean due to the prevailing strong southwesterly winds (~30 knots) off the Moroccan coasts. Similar synoptic conditions have been presented in Cluster 2 in Gkikas et al., (2015), who studied the atmospheric circulation evolution related to the occurrence of desert dust episodes over the Mediterranean.

At a first glance, it is evident that the DRE patterns are driven by those of the desert dust outbreaks whereas small scale isolated features of extremely high/low DREs mainly result from slight “shifts” of clouds between the two independent model runs. Moreover, it is apparent that both the sign and the magnitude of DREs vary among TOA, surface and atmosphere as well as with time (day or night). It must be mentioned that the limits of the DREs’ colorbars in Figure 4 are set equal to -300 and 300 Wm^{-2} in order to facilitate the intercomparison among the different levels within the Earth-Atmosphere system, the comparison between day and night DREs and the visualization of our results. During daytime (12 h and 36 h) the DREs are driven by their SW components which significantly exceed the LW ones. Through absorption and scattering of solar radiation by mineral particles, the downwelling radiation at the ground (SURF) is reduced by up to 308 Wm^{-2}, indicating a strong surface cooling (bluish colors) in areas where the dust AOD is maximized like Mauritania or south Algeria. During nighttime (24 h and 48 h), the sign of the DRE_{SURF} values is reversed and their magnitude decreases compared to that at 12 h and 36 h. This is because during the night the DRE_{SURF} values are identical to the LW DRE ones, which are positive, implying extra downwelling LW radiation at the surface, by up to 58 Wm^{-2}, emitted by the overlying dust. This effect, leading to night surface warming, is more visible over specific parts of Sahara that host high dust loads, e.g. in its western parts. The geographical patterns of $DRE_{NETSURF}$ are very similar to those of DRE_{SURF}, as expected, since they only differ by the net upward radiation at the surface, which in turn is determined by surface albedo and temperature. DRE for NETSURF expresses the amount of radiation absorbed at the ground and is calculated through the subtraction of the upward from the downward surface radiative fluxes (see Eq. 3). Therefore, the differences between DRE_{SURF} and $DRE_{NETSURF}$ are regulated by the upward component, which in turn is determined by the surface albedo and temperature for the SW and LW radiation, respectively. For this reason, the negative differences (i.e. DRE_{SURF}-$DRE_{NETSURF}$) at noon are maximized over highly reflective areas, while the positive ones at night are observed in land areas where the surface cooling during sunlight hours is maximized (i.e. reduction of the surface temperature during day leads to reduction of the emitted longwave radiation during night). Based on our results, the negative (surface cooling) and positive (surface warming) $DRE_{NETSURF}$ values can reach down to -290 Wm^{-2} (eastern Atlantic Ocean) and up to 42 Wm^{-2} (western Sahara) during day and night, respectively. Among our studied cases (see Table S1) the instantaneous NET DRE_{SURF} and $DRE_{NETSURF}$ values at noon can be as large as -589 Wm^{-2} and -337 Wm^{-2}, respectively, in agreement with relevant results reported in previous studies dealing with the radiative impacts of dust intrusions in the Mediterranean (Pérez et al, 2006; Remy et al., 2015), in west Africa (Heinold et al., 2008; Mallet et al., 2009) and in Asia (Wang et al., 2009; Singh and Beegum et al., 2013).

The occurrence of desert dust outbreaks results in a strong perturbation of the atmospheric radiation budget, attributed to the interaction of dust aerosols with the SW and LW radiation. More specifically, during daytime (i.e. 12 h and 36 h), mineral particles absorb radiation at short wavelengths warming thus the atmosphere as indicated by the positive instantaneous NET DRE_{ATM} values in Figure 4 (third column), reaching up to 189 Wm^{-2} over the dust affected areas. Our calculated noon atmospheric DREs (Table S1) are comparable to those reported by Heinold et al. (2008; 2011) and significantly lower compared to those in Pérez et al. (2006), who found DRE_{ATM} values higher than 500 Wm^{-2} in land areas with dust AOD > 3 during a desert outbreak that affected the Mediterranean on 12th April 2002. We note that Pérez et al., (2006) used complex refractive indices taken from the Global Aerosol Data Set (GADS) that have been shown to be excessively absorbing, which may partly explain their high DRE_{ATM} values. In order to highlight the strong instantaneous atmospheric warming induced by the desert dust outbreaks, we have compared our results with similar ones obtained by previous studies that have been relied on long-term model simulations. Zhao et al., (2011) found that the average net atmospheric warming across the Sahara Desert, over the period April-September 2006, can be higher than 30 Wm^{-2} based on regional simulations of the WRF-Chem model. According to global simulations conducted at climatic scales (e.g. Woodage and Woodward, 2014), dust aerosols can increase the absorbed radiation into the atmosphere (warming effect) by up to 20 Wm^{-2} across the Northern Africa. Radiative transfer computations of SW DRE_{ATM} for the 2000-2007 period by Papadimas et al. (2012) reported local values of a few decades up to about 100 Wm^{-2} in spring and summer above the Sahara Desert. During night, negative DRE_{ATM} values (down to -45 Wm^{-2} in Algeria and Mali) are computed in the dust affected areas indicating an atmospheric cooling because of the emission of LW radiation by mineral particles (Wang et al., 2013b).

The sign and magnitude of DRE_{TOA} (Eq. 4) are regulated by $DRE_{NETSURF}$ and DRE_{ATM}. At noon and above cloud-free areas, there is a distinct change of DRE_{TOA} sign over oceanic and desert areas affected by dust loads (note for example the red colors over the dusty western Sahara Desert regions, e.g. Mauritania, against blue colors off the African coasts). This change of the DRE_{TOA} sign is due to the difference in surface albedo of the two types of surface (water and desert), in combination with dust high AODs and low-to-moderate single scattering albedo enhancing solar absorption by dust above highly multiple reflecting surfaces. Such a reverse of DRE_{TOA} sign has been also reported in previous studies (e.g. Santese et al., 2010; Nabat et al., 2012; Papadimas et al., 2012) and is characterized by a clear contrast between red and blue colors (planetary warming and cooling, respectively) over adjacent continental and oceanic areas. Over highly reflective surfaces (i.e. deserts), the atmospheric warming is enhanced since dust aerosols absorb not only the incoming solar radiation but also the radiation reflected by the surface. At the same time, the amount of the absorbed radiation at the ground is reduced by the attenuation of the SW radiation and by the increase of the back reflected radiation at the surface. The combination of these processes results in a predominance of the atmospheric warming over surface cooling and subsequently to positive DRE_{TOA} values (planetary warming), which can be as large as 85 Wm^{-2} according to our simulations (Table S1). On the contrary, when dust aerosols are suspended over dark surfaces (i.e. maritime areas), the condition is reversed and negative DRE_{TOA} values down to -184 Wm^{-2} (Table S1) are calculated, revealing thus a strong planetary cooling. Nevertheless, the positive DRE_{TOA} values exceeding 300 Wm^{-2}, which are recorded in maritime areas off the western African coasts, are associated with the existence of absorbing dust aerosols superimposed over low- and mid-level clouds. During night, the atmospheric cooling offsets the surface warming, both induced by the desert dust outbreaks, and for this reason the DRE_{TOA} values are almost negligible (do not exceed 10 Wm^{-2} in absolute terms over cloud free areas) indicating an almost null dust direct radiative effect. Our model computed dust induced planetary warming above western Africa is comparable to similar results reported in previous studies focusing on the same or similar desert areas (e.g. Mallet et al., 2009; Pérez et al., 2006; Wang et al., 2010; Nabat et al., 2012; Kalendeski and Stenchikov et al., 2016), although differences also exist with regards to the magnitude or spatial DRE_{TOA} patterns. These differences are attributed to the different magnitude and spatial patterns of AOD values (dust loads) associated with the different studied dust outbreaks, and also to differences in dust microphysical and optical properties (Colarco et al., 2014).

5.2.2. Regional mean results

In order to show more clearly temporal patterns, DREs were also averaged over the NSD (outer NMMB Simulation Domain in Figure 1), SDD (Sahara Desert Domain, green rectangle in Figure 1) and MSD (Mediterranean Satellite Domain, red rectangle in Figure 1) domains, for each desert dust outbreak, separately for the NET, SW and LW radiation. Only cloud free grid points, in both model configurations (RADON and RADOFF), with RADON dust AOD_{550nm} values higher/equal than 0.05 have been considered in this analysis. Then, in a further step, DRE values have been averaged over the 20 dust outbreaks every three hours during the forecast period (84 hours). Thus, the time series of regional mean and associated standard deviation (shaded areas) clear-sky TOA (black curve), SURF (purple curve), NETSURF (blue curve) and ATM (red curve) DREs are depicted in Figure 5.

The SW clear-sky DREs (upper row in Fig. 5) are positive in the atmosphere (ATM, warming effect) and negative at the surface (SURF and NETSURF, cooling effect) throughout the entire forecast period, revealing a distinct diurnal cycle with marked maximum values around noon over all three domains. A careful look, however, reveals some differences between the sub-regions. Thus, in NSD (first column) and SDD (second column) the maximum DRE_{ATM} values increase slightly with time from 30 to 35 Wm^{-2}, while in contrast they decrease in MSD (third column) from 30 to 22 Wm^{-2}. Respectively, the negative DRE_{SURF} values (surface cooling) reach down to -50 Wm^{-2} in the NMMB and the Sahara domain while in the Mediterranean area reach down to -57 Wm^{-2}. In addition, the magnitude of DRE_{SURF} and $DRE_{NETSURF}$ values in NSD and SDD do not change with time, against a slight decrease in MSD to -40 Wm^{-2}. Hence, our results show that during the first 36 forecast hours, the computed DRE_{SURF} and $DRE_{NETSURF}$ values in MSD are larger than in SDD, while SDD is the source area of dust outbreaks. This can be explained by the fact that the massive dust loads originating across the Sahara "enter" very fast the Mediterranean domain leading thus to higher dust AODs (Figure S2) and larger reductions of surface solar radiation (DRE_{SURF} and $DRE_{NETSURF}$ values). Another possible explanation can be the variability of dust loads' intensity across Sahara (SDD) and Mediterranean (MSD). In the former region, mineral particles' loads are maximum but there are many grid points in which the simulated dust AODs are equal or slightly higher than the required threshold (0.05). Therefore, the regional averages of DREs in SDD are "smoothed" in contrast to MSD, where the number of grid points participating in the regional calculations of DREs, although is lower, moderate-to-high dust AODs are forecasted there. As it concerns the SW $DRE_{NETSURF}$ values, their temporal variation is identical to the corresponding ones for DRE_{SURF}; however, the former ones are lower by up to 15 Wm^{-2}, in absolute terms. The most noticeable difference between the two sub-domains (i.e. SDD and MSD) is encountered for the DRE_{TOA} at noon. Over bright desert surfaces, dust outbreaks warm the Earth-Atmosphere system as indicated by the positive DRE_{TOA} values (up to 3.2 Wm^{-2}) while over the darker (mostly covered by sea) surfaces of the Mediterranean, the mineral particles induce a planetary cooling with DRE_{TOA} values ranging from -20 to -10 Wm^{-2}. In both subdomains, the strongest planetary cooling is found at early morning and afternoon hours with negative SW DRE_{TOA} values down to -14.1 Wm^{-2} and -25.1 Wm^{-2} over Sahara and Mediterranean, respectively. On the contrary, DRE_{TOA} values decrease towards noon, due to increasing solar absorption and decreasing scattering by dust under smaller solar zenith angles. Finally, due to the gradually decreasing desert dust outbreaks' intensity within the MSD (Figure S2-i) for increasing forecast time, their radiative impacts at all levels of the Earth-Atmosphere system are reduced as well in contrast to slightly increased values in SDD.

The regional clear-sky DREs have been also computed for the LW spectrum (middle row in Figure 5) revealing reverse effects of lower magnitude (in absolute terms) with respect to the corresponding ones found at short wavelengths. Due to the emission of LW radiation by the mineral particles, desert dust outbreaks induce an atmospheric cooling (negative LW DRE_{ATM} values) and increase the amount of the downward LW radiation at the surface (positive LW DRE_{SURF} values). Both DRE_{ATM} and DRE_{SURF} levels do not reveal remarkable temporal variation ranging from -4.8 to -2.8 Wm^{-2} and from 1.9 to 4.3 Wm^{-2}, respectively, in the NSD and SDD while slightly lower values are calculated for the MSD. On the contrary, from the timeseries of the LW DREs for TOA and NETSURF it is evident the existence of a diurnal cycle with maximum and minimum values around noon and during nighttime, respectively. Moreover, both DRE_{TOA} and $DRE_{NETSURF}$ values are higher than zero, throughout the simulation period, indicating a warming LW radiative effect. More specifically, regional LW DRE_{TOA} ranges from 0.1 to 3.4 Wm^{-2} and $DRE_{NETSURF}$ varies between 2.9 and 8 Wm^{-2} for the whole simulation domain (NSD). The corresponding maximum DREs for the SDD and MSD are higher by up to 0.5 Wm^{-2} and lower by up to 1.2 Wm^{-2}, respectively. Dust aerosols act like greenhouse gases (Miller and Tegen, 1998) trapping the outgoing terrestrial radiation while at the same time emit radiation at longer wavelengths back to the ground explaining thus the positive LW DREs for TOA (planetary warming) and NETSURF (surface warming). In addition, the aforementioned LW DREs (TOA and NETSURF) covariate with time revealing that the sign and the magnitude of the LW DRE_{TOA} are determined by the perturbation of the surface radiation budget (LW $DRE_{NETSURF}$) since the LW DRE_{ATM} values are almost constant throughout the simulation period. This is in contrast to the corresponding finding for the SW radiation where the dust outbreaks' impact on the Earth-Atmosphere system's radiation budget is regulated by the perturbation of the radiation fields into the atmosphere (ATM) and at the surface (NETSURF). Finally, between SDD and MSD stronger LW DREs are found for the former domain due to the higher dust loads over the Sahara as well as due to the larger size of mineral particles close to the source areas.

As it has been shown from the above analysis, the dust DREs between short and long wavelengths are reverse (except at TOA over the Sahara around midday) and in order to assess the impact of desert dust outbreaks in the whole spectrum the regional clear-sky NET (SW+LW) DREs have been also analyzed (bottom row in Fig. 5). During sunlight hours, the NET DREs result from the compensation of the SW and LW effects while during night the NET and the LW DREs are equal attributed to the absence of SW radiation. Based on our results, in the NSD, the DRE_{TOA}, DRE_{SURF}, $DRE_{NETSURF}$ and DRE_{ATM} range from -13.9 to 2.6 Wm^{-2}, from -43.6 to 4 Wm^{-2}, from -26.3 to 3.9 Wm^{-2} and from -3.7 to 28 Wm^{-2}, respectively. In the SDD, the corresponding NET DREs vary from -11.9 to 7.1 Wm^{-2}, from -46.3 to 4.3 Wm^{-2}, from -24.7 to 4.2 Wm^{-2} and from -4.1 to 30.2 Wm^{-2}, respectively. Over the Mediterranean, the DREs for TOA range from -23.7 to 0.9 Wm^{-2}, for SURF from -53.5 to 4.1 Wm^{-2}, for NETSURF from -39.4 to 4.2 Wm^{-2} and for ATM from -4 to 25.5 Wm^{-2}. Moreover, due to the reduction of the desert dust outbreaks' intensity for increasing forecast hours (Figure S2-i) the associated direct radiative effects are also reduced within the MSD.

At noon, the SW planetary cooling counterbalances the LW planetary warming resulting thus to almost zero DRE_{TOA} values (null effect) over the whole simulation domain (NSD). On the contrary, in the SDD, both SW and LW DRE_{TOA} are positive due to the higher surface albedo and the trapping of the surface upward LW radiation by mineral particles, respectively, leading to a net warming of the Earth-Atmosphere system. In the broader Mediterranean area (MSD), the SW effects at TOA (planetary cooling) dominate over the corresponding effects at longer wavelengths (planetary warming) explaining thus the negative NET DRE_{TOA} values (planetary cooling). In the atmosphere, for the three domains, the negative LW DREs offset by about 12-14% the positive SW ones resulting to an overall warming effect (positive NET DRE_{ATM}) around midday. Moreover, at noon, the increase of the absorbed LW radiation at the ground offsets the decrease of the absorbed SW radiation by about 20-24% resulting in a NET surface cooling (negative NET $DRE_{NETSURF}$) over the simulation domain. The corresponding levels for the SDD and MSD vary from 25 to 28% and from 14 to 15%, respectively. In addition, the increase of the downwelling LW radiation at the ground offsets by up to 8% the decrease of the downward SW radiation resulting in negative NET DRE_{SURF} values across the Sahara Desert (i.e. SDD).

Beyond the hourly and day-to-day variability of dust DREs, the results were averaged over the total 84-hour simulation period and the results are given, for the three domains, in Table 2, separately for the SW, LW and NET radiation. The results are similar for the three domains, as to their physical meaning, i.e. dust produces a SW cooling/heating of surface/atmosphere, resulting in a planetary SW cooling, against a LW heating/cooling of surface/atmosphere, yielding a planetary LW heating. At TOA, desert dust outbreaks cause a net planetary cooling with clear-sky NET DRE_{TOA} values equal to -3.4±5.6, -1.6±6.1 and -8.2±8.2 Wm^{-2} for the NSD, SDD and MSD, respectively. Note, that due to the very strong temporal variability of DREs at TOA, the computed standard deviations are considerably higher than the averages in the NSD and SDD in contrast to MSD where are equal. Yoshioka et al., (2007), based on long-term simulations, reported a negative DRE_{TOA} (-4.73 Wm^{-2}) averaged over North Africa (mean dust AOD equal to 0.39) and Heald et al. (2014) found that the all-sky NET DRE_{TOA} values vary from -3 to 4 Wm^{-2} across the Sahara for the year 2010. Woodage and Woodward (2014) and Zhao et al., (2011) calculated positive DREs at TOA, averaged for the northwestern Africa, equal to 4.74 Wm^{-2} and 0.83 Wm^{-2}, respectively. The negative averaged NET DRE_{TOA} in SDD is attributed to the planetary cooling found at early morning and afternoon hours. Wang et al. (2011) showed that when solar altitude is low (i.e. high solar zenith angle) DRE at TOA is getting negative even over high-albedo deserts. Similar results reported also by Banks et al. (2014), who studied the daytime cycle of dust DREs during the Fennec campaign held in the central Sahara in June 2011. Our results for the DRE_{TOA} in the MSD are within the ranges reported in previous studies (e.g. Valenzuela et al., 2012; Sicard et al., 2014a;b) dealing with dust intrusions in the Mediterranean. From the comparison of the SW and LW DRE_{TOA}, it is found that the LW planetary warming offsets the SW planetary cooling by 33.3% in the NSD, by 52.9% in the SDD and by 15.4% in the MSD. In the atmosphere, mineral particles cause an overall atmospheric warming with NET DRE_{ATM} levels varying from 7.3±11 (MSD) to 8.3±13 Wm^{-2} (SDD) while the offset of the SW atmospheric warming by the LW atmospheric cooling ranges from 31.1% to 33.6% among the study domains. On an average, dust outbreaks reduce the downwelling NET radiation at the ground (DRE_{SURF}) by up to -20.7±21.6 Wm^{-2} (NSD), -20.1±21.9 Wm^{-2} (SDD) and -22.7±23.6 Wm^{-2} (MSD) while the corresponding $DRE_{NETSURF}$ levels are equal to -11.6±13.4 Wm^{-2}, -9.9±12.4 Wm^{-2} and -15.6±17.5 Wm^{-2}, respectively. Our results for the SW and LW radiation in the SDD are in a good agreement with the annual averages for the year 2008 presented by Nabat et al. (2012) over Northern

Africa. Santese et al. (2010), for a similar domain, calculated higher daily averages of regional SW and LW $DRE_{NETSURF}$ values by up to 8 and 3 Wm^{-2}, respectively, for two dust outbreaks that took place on 17^{th} and 23^{rd} July 2003. For the DRE_{SURF}, the ratio of the LW/SW effects does not exceed 15.2% (SDD) while the corresponding ratios for the $DRE_{NETSURF}$ are minimum for the MSD (23.5%) and maximum for the SDD (37.7%). From the above analysis it is clear that dust outbreaks' impact at short wavelengths is more pronounced than in the longwave spectrum; however, the contribution of the LW DREs to the NET ones is significant or even larger, particularly over the Sahara at midday.

5.3. Impact on sensible and latent heat fluxes

As it has been shown in previous section, dust outbreaks exert a strong perturbation of the surface radiation budget by reducing and increasing the absorbed NET radiation at the ground during day and night, respectively. As a response to these disturbances, the surface heat fluxes, both sensible (SH) and latent (LE), associated with the transfer of energy (heat) and moisture between surface and atmosphere, also change in such a way trying to balance the gain or the loss of energy at the ground (Miller and Tegen, 1998). Subsequently, variations of SH and LE have impact on the components of the hydrological cycle (Miller et al., 2004b) as well as on the turbulent kinetic energy and momentum transfer which in turn affect near surface winds and dust emission (Pérez et al., 2006). Moreover, Marcella and Eltahir (2014) and Kumar et al. (2014) have shown that due to the presence of dust aerosols into the atmosphere, the daytime surface sensible heat fluxes are reduced leading to a reduction of the planetary boundary layer (PBL) height.

Here, we are investigating the impact of desert dust outbreaks on SH and LE over the simulation domain. It must be clarified that our analysis is restricted only above land areas since we are looking at short-term effects and also in the existing version of the NMMB-MONARCH model the atmospheric driver is not coupled with an ocean model. The time series of the regional SH and LE values, over the forecast period, based on the RADON (red curve) and RADOFF (blue curve) configurations of the model are presented in Figures 6-i (for SH) and 6-ii (for LE). Each curve corresponds to the mean levels calculated from the 20 desert dust outbreaks while the shaded areas represent the associated standard deviations. According to our results, SH is characterized by a diurnal variation with maximum values (~ 350 Wm^{-2}) at noon and minimum ones (~ -30 Wm^{-2}) during nighttime (Fig. 6-i). Nevertheless, during sunlight hours, the surface sensible heat fluxes simulated in the RADON experiment are lower by up to 45 Wm^{-2} in comparison to the RADOFF outputs. At night, an opposite tendency is recorded and the

RADON SH fluxes are higher by up to 2 Wm^{-2} than the corresponding fluxes based on the RADOFF configuration of the model. The reverse effects on SH levels, over the western parts of the Sahara, between daytime and nighttime as well as the diurnal variability of their magnitude have been pointed out by Zhao et al. (2011). Based on the paired t-test, the differences between RADOFF and RADON SH values are statistical significant at 95% confidence level throughout the forecast period. At local scale (geographical distributions), among the studied cases, in areas where the desert dust outbreaks' intensity is maximized, the SH fluxes are reduced by up to 150 Wm^{-2} during day and increased by up to 50 Wm^{-2} during night. Our findings are consistent with those presented by Mallet et al. (2009) and Rémy et al. (2015) who analyzed the impact of dust storms on sensible heat fluxes over W. Africa and Mediterranean, respectively, and substantially higher than the instantaneous perturbations of SH calculated by Kumar et al. (2014), who studied a dust outbreak that occurred in northern India (17-22 April 2010).

The diurnal variation of the latent heat fluxes (Fig. 6-ii) is identical to that of sensible heat fluxes; however, LE levels are remarkably lower than the regional averages of SH. This is attributed to the lower soil water content and limited evaporation in arid regions leading thus to a predominance of the sensible heat fluxes (Ling et al., 2014). Based on our simulations, LE values at noon gradually decrease both for the RADOFF (blue) and RADON (red) experiments over the forecast period probably attributed to the too moist initialization of the model (Note that the model is initialized with FNL analysis produced by a different model (GFS)). Nevertheless, the latter LE values are lower than the former ones by up to 4 Wm^{-2} indicating that desert dust outbreaks reduce the latent heat fluxes leaving from the ground. The reliability of this finding is further supported by the fact that the RADOFF-RADON differences are statistically significant at 95% confidence level. During night, the RADON LE values are slightly higher (less than 0.5 Wm^{-2}) with respect to the corresponding ones simulated in the RADOFF configuration. The instantaneous reduction and increase of LE (results not shown here) are substantially higher than the regional perturbations and can be as large as -100 Wm^{-2} and 20-30 Wm^{-2}, respectively. Finally, in contrast to SH, the spatial features of LE anomalies are not identical with those of $DRE_{NETSURF}$ since other parameters (e.g. soil moisture) regulate also the latent heat fluxes (Marcella and Eltahir, 2014).

5.4. Impact on temperature fields

Through the perturbation of the radiation by the mineral particles it is expected that desert dust outbreaks will affect also the temperature fields. In order to quantify these impacts, the temperature differences between the RADON and RADOFF simulations, both at 2 meters and in vertical, are analyzed. In Figure 7, are displayed the RADON-RADOFF anomaly maps of temperature at 2 meters at

12 (i), 24 (ii), 36 (iii) and 48 (iv) hours after the initialization of the forecast period on 2nd August 2012 at 00 UTC. At noon, the highest negative biases (down to -4 K) are observed over land areas where the intensity of dust loads is high (see the first and third row in the first column in Fig. 4) due to the strong reduction of the NET radiation reaching the ground by the mineral particles. Similar findings, under dust episode conditions, have been also reported by previous studies conducted for the Mediterranean (Pérez et al., 2006), across the Sahara (Helmert et al., 2007; Heinold et al., 2008; Stanelle et al., 2010) and in East Asia (Kumar et al., 2014; Ling et al., 2014). Over dust-affected maritime areas, due to the higher heat capacity of the sea, the temperature differences between the RADON and RADOFF experiments are almost negligible at these time scales. During nighttime, dust aerosols emit radiation at thermal wavelengths increasing thus the near surface temperature when the dust-radiation interactions are included into the numerical simulations (RADON experiment). For this reason, the RADON-RADOFF temperature differences at 2 meters become positive (up to 4 K) at 24 and 48 forecast hours over land areas where the "core" of the dust plume is observed. The reduction and the increase of the near surface temperature during daytime and nighttime, respectively, either solely or as a combined result indicate that the temperature diurnal range is reduced due to desert dust outbreaks.

The vertical distribution of dust layers determines their impacts on radiation with altitude which in turn modify the temperature profiles (Meloni et al., 2015) and subsequently affect convection (Ji et al., 2015), cloud development (Yin and Chen, 2007), precipitation (Yin et al., 2002) and wind profiles (Choobari et al., 2012). In order to investigate the impacts of desert dust outbreaks on temperature fields into the atmosphere, we have reproduced the altitude-latitude cross sections (up to 8 km above mean sea level, m.s.l.) of RADON-RADOFF temperature differences on 4 April 2003 at 12 UTC along the meridional 30° E (Fig. 8 ii-a) and on 7 March 2009 at 00 UTC along the meridional 10° E (Fig. 8 ii-b). In addition, the corresponding cross sections of dust concentration (in kg m^{-3}) are shown in Figures 8 i-a and 8 i-b, respectively. At midday, an elevated dust layer extends from 1.5 to 6 km m.s.l., between 23° N and 33° N, with dust concentrations up to 0.8×10^{-6} kg m^{-3} while a low elevated dust layer extends from the surface up to 1.5 km m.s.l., between 27° N and 31° N, with concentrations up to 10^{-6} kg m^{-3} (Fig 8 i-a). Based on the cross section of temperature differences (Fig. 8 ii-a), dust aerosols via the absorption of solar radiation warm the atmospheric layers by up to 0.8-0.9 K between altitudes where the high-elevated dust layer is located. On the contrary, below the dust cloud, mineral particles cool the lowest tropospheric levels (by up to 1.3 K) by attenuating (through scattering and absorption) the incoming solar radiation. Note that between the parallels 31° N and 35° N, where dust loads are recorded at low altitudes (below 2 km), higher temperatures by up to 0.3 K are simulated in the RADON experiment with respect to

RADOFF, revealing thus an atmospheric warming near surface. Also, it must be considered that in this area mineral particles are suspended over sea, where the impacts on sensible heat fluxes are negligible, making therefore evident the dust warming effect at low atmospheric levels in contrast to land areas (parallels between 27° N and 31° N), where the near surface temperature is reduced because of the reduction of the sensible heat fluxes, as it has been shown also by Pérez et al. (2006, Fig. 10). Therefore, the vertical distribution of dust loads plays a significant role regarding their impact on near surface temperature which in turn may affect winds and subsequently dust emission (Stanele et al., 2010; Huang et al., 2014). Above the high-elevated dust layer, negative RADON-RADOFF temperature differences (down to -0.3 K) are found indicating an atmospheric cooling attributed to the dust albedo effect (Spyrou et al., 2013).

In the second example, on 7th March 2009 at 00 UTC, a dust layer extends from the southern parts of the NSD domain to the northern parts of Tunisia, between surface and 4 km m.s.l. (Fig. 8 i-b). Along the dust plume, moderate concentrations (up to 0.5×10^{-6} kg m^{-3}) are simulated between 15° N and 20° N, low (less than 0.2×10^{-6} kg m^{-3}) between 20° N and 25° N while the maximum ones (higher than 2×10^{-6} kg m^{-3}) are recorded between 25° N and 35° N. Due to the emission of LW radiation by mineral particles, dust aerosols cool the atmospheric layers (Otto et al., 2007) in which they reside, by up to 0.8 K, and increase the temperature, by up to 0.4 K, just above the dust layer. Between the bottom of the dust layer and surface, positive RADON-RADOFF temperature differences (i.e. warming) up to 1.2 K are calculated as indicated by the red colors following the model topography (grey shaded). Mineral particles emit LW radiation and trap the outgoing terrestrial radiation explaining thus the warming effect of dust outbreaks close to the ground during nighttime. Nevertheless, this near surface warming is “interrupted”, being null or even reverse (i.e. cooling), in areas where the dust layer abuts the ground.

5.5. Feedbacks on dust emission and dust aerosol optical depth

In the present section, focus is given on the investigation of the potential feedbacks on dust AOD (at 550 nm) and dust emissions attributed to dust radiative effects. To this aim, the timeseries of the regional averages and the associated standard deviations, throughout the forecast period (84 hours), calculated from the 20 desert dust outbreaks for both parameters, based on the RADON (red) and RADOFF (blue) experiments, are analyzed and the obtained results are shown in Figure 9. Over the simulation period, the RADOFF dust AOD_{550nm} gradually increases from 0.31 to 0.34 in contrast to the corresponding outputs from RADON that are gradually decreasing down to 0.29 (Fig. 9-i). The positive RADOFF-RADON differences of dust AOD, indicating a negative feedback when the dust-radiation interactions are considered into the numerical simulations, are getting evident 12 hours (0.005 or 2%) after the initialization of the forecast period and amplify with time (up to 0.036 or 12%), being also statistical significant (paired t-test, confidence level at 95%) at each forecast step. The observed negative feedbacks on dust AOD have been also pointed out in relevant studies carried out for specific desert dust outbreaks; however, the reductions of mineral particles' loads were significantly higher compared to our calculations corresponding to averages of the 20 studied desert dust outbreaks. More specifically, Pérez et al. (2006) found a reduction of the regional dust AOD by up to 35-45 % and in Wang et al. (2010) the corresponding reductions were ranging between 10 and 45%. Through the comparison of the mean dust AOD levels, calculated over the 84-h simulation period, based on RADON (0.288) and RADOFF (0.308) simulations, it is revealed a statistical significant reduction by 0.02 (6.9 %) attributed to the dust radiative effects. Among the 20 desert dust outbreaks, these reductions vary from 1% (22 February 2004) to 12.5% (27 January 2005) and are statistical significant at 95 % confidence level in all cases.

A similar analysis has been also made for the dust emissions (in kg m^{-2}) aggregated over the whole simulation domain (NSD, outer domain in Figure 1). First, for each case and in each forecast step, the dust emissions from all grid points within the NSD are aggregated. Then, the mean and the standard deviation values are computed from the 20 desert dust outbreaks which are analyzed and the overall results are given in Figure 9-ii. Moreover, the total dust emissions at each forecast step are added and the obtained results, separately for the RADON and RADOFF configuration of the model, are provided into the parentheses in the legend of Figure 9-ii. Dust emissions are maximized around midday (Cowie et al., 2014) and are very weak during night. Based on the RADOFF simulation, the highest amounts of emitted dust are increased from 2 to 2.5 kg m^{-2} throughout the hindcast period. This increasing tendency is encountered also in the RADON experiment; however, the dust emission is lower compared to the simulation in which the dust-radiation interactions are neglected (RADOFF). The positive RADOFF-RADON anomalies during daytime range from 0.1 to 0.4 kg m^{-2} and are statistical significant at 95% confidence level based on the paired t-test. Therefore, desert dust outbreaks exert a negative feedback on dust emission explaining thus the reduction of dust AOD. The lower amounts of emitted dust, modelled based on the RADON configuration, result from a chain of processes triggered by the surface cooling which decreases the turbulent flux of sensible heat into the atmosphere, weakening the turbulent mixing within the PBL and the downward transport of momentum to the surface and subsequently reduces surface wind speed and dust emission (Miller et al., 2004a; Pérez et al., 2006).

During the simulation period, the total emitted amount of desert dust is equal to 18.279 and 21.849 kg m^{-2} based on the RADON and RADOFF, respectively. Therefore, desert dust outbreaks cause a negative feedback on dust emissions reducing them by 3.57 kg m^{-2} (-19.5%). This reduction (i.e. positive RADOFF-RADON differences) is consistent in all the studied cases of our analysis varying from 0.6 kg m^{-2} (~10%, 24 February 2006) to 6.6 kg m^{-2} (~34%, 2 August 2012). Negative feedbacks on dust AOD and dust emissions have been also pointed out in previous studies based on short- (e.g. Ahn et al., 2007; Rémy et al., 2015) and long-term (e.g. Perlwitz et al., 2001; Zhang et al., 2009) simulations. Woodage and Woodward (2014) relied on climatic simulations of the HiGEM model, found a positive feedback on global dust emissions which is in contradiction with findings reported in the majority of the existing studies. The authors claimed that this discrepancy could be explained by the absence of mineral particles with a radius larger than 10 μm in the emitted dust size distribution leading thus to an underestimation of the LW effects. It must be clarified that according to our results negative feedbacks on dust emission are found at a regional scale. Stanelle et al. (2010) showed that the vertical distribution of dust aerosols determines their impacts on atmospheric stability and wind patterns and subsequently the associated feedbacks on dust emissions which can be even positive at a local scale. This highlights the importance of studying the potential feedbacks on mineral particles' loads as well as on their emissions spatially by analyzing all the contributor factors.

5.6. Assessment of the radiation at the ground

The performance of the NMMB-MONARCH model in terms of reproducing the downward SW and LW radiation is assessed using as reference data ground measurements derived from the Baseline Surface Radiation Network (BSRN, Ohmura et al., 1998), a project of the Data and Assessments Panel from the Global Energy and Water Cycle Experiment (GEWEX, http://www.gewex.org/) under the umbrella of the World Climate Research Programme (WCRP, https://www.wcrp-climate.org/). Through this analysis it is attempted to quantify objectively the potential improvements of the model's predictive skills attributed to the inclusion of the dust radiative effects into the numerical simulations. Globally, 59 BSRN stations are installed at different climatic zones providing radiation measurements (http://bsrn.awi.de/) of high accuracy at very high temporal resolution (1 min) (Roesch et al., 2011). For the evaluation analysis, we have used the global (direct and diffuse) shortwave and longwave downwelling radiation at the ground measured at 6 stations (magenta star symbols in Figure 1) located in Spain (Izana, Cener), France (Palaiseau, Carpentras), Algeria (Tamanrasset) and Israel (Sede Boker).

In Figure 10, are presented the timeseries of the measured (red curve) SW (i-) and LW (ii-) radiation at Sede Boker and the corresponding model outputs based on the RADON (black curve) and the RADOFF (blue curve) experiments, for the periods 22 February 2004 00 UTC – 25 February 2004 12

UTC (-a) and 21 April 2007 00 UTC – 24 April 2007 12 UTC (-b). In the bottom row of Fig. 10 are also provided the temporal evolution of the model dust AOD_{550nm} and the Level 2 AERONET total AOD_{500nm} (red x symbols) retrieved via the O' Neill algorithm (O' Neill et al., 2003). Moreover, the AERONET Ångström exponent (alpha) retrievals (denoted with green x symbols) are used as an indicator of coarse or fine particles predominance into the atmosphere. For the comparison between model and observations, the nearest grid point (minimum Euclidean distance) to the stations' coordinates is utilized. In Sede Boker, the model's grid point elevation is 465 m being slightly lower than the AERONET (480 m) and BSRN (500 m) stations, and therefore these small altitude differences do not affect substantially the intercomparison results. Likewise, the SW and LW radiation are measured from 0.295 to 2.8 μm and from 4 to 50 μm, respectively, while the spectral intervals in the model's radiation transfer scheme span from 0.2 to 12.2 μm and from 3.3 to 1000 μm in the shortwave and longwave spectrum, respectively. These differences might contribute to the level of agreement between model and observations; however, are not discussed in our evaluation analysis.

In both examples presented here, but also for the rest of our dataset, the model captures better the temporal variation of the downwelling SW in contrast to the LW radiation at the ground with correlation coefficients (R) higher than 0.96 and between 0.63 and 0.85, respectively. However, the model-BSRN biases vary strongly in temporal terms because of the inability of the model to reproduce adequately the amount of the suspended mineral particles. For the first desert dust outbreak (left column in Fig. 10), during the first forecast day, the maximum measured SW radiation is higher by about 150 Wm^{-2} than the simulated RADON outputs and slightly lower than the corresponding RADOFF levels. The former is explained by the facts that the model reproduces the dust peak earlier than actually recorded according to AERONET observations (see Figure 10 iii-a) and it develops low-level clouds (cloud fractions between 0.5 and 0.6) while the latter one is attributed to the absence of dust radiative effects. For the rest of the simulation period, the model overestimates and underestimates the shortwave and longwave radiation, respectively, due to its deficiency to reproduce (underestimation) the amount of dust aerosols. More specifically, based on AERONET retrievals, AOD and alpha levels vary from 0.2 to 0.4 and from 0.2 to 0.7, respectively, indicating the existence of dust loads of moderate intensity. On the contrary, the simulated dust AOD at 550 is less than 0.1 in both model configurations characterized by a "flat" behavior in temporal terms. Over the simulation period (22 February 2004 00 UTC – 25 February 2004 12 UTC), the mean SW (LW) radiation based on BSRN, RADON and RADOFF is equal to 221.6 Wm^{-2} (290.0 Wm^{-2}), 255.4 Wm^{-2} (266.4 Wm^{-2}) and 272.7 Wm^{-2} (264.7 Wm^{-2}), respectively. Thanks to the consideration of the dust radiative effects, the positive model-BSRN biases in the shortwave spectrum are reduced from 51.1 Wm^{-2} (RADOFF-BSRN) to 33.9 Wm^{-2} (RADON-BSRN) while the negative model-BSRN biases in the longwave spectrum are reduced from -25.3 Wm^{-2} (RADOFF-BSRN) to -23.6 Wm^{-2} (RADON-BSRN).

In the second case which is analyzed (right column in Fig. 10), two peaks are simulated with dust AOD_{550nm} values up to 0.9 (midday on 23rd April 2007) and 0.5 (afternoon on 21st April 2007). For the major one, the model clearly overestimates aerosol optical depth with respect to AERONET retrievals in which AOD (red x symbols) varies between 0.2 and 0.3 and alpha (green x symbols) ranges from 0.3 to 0.5 while the second one cannot be confirmed due to the lack of ground observations. Note, that between 09 UTC and 15 UTC on 23rd April 2007, the model underestimates the SW radiation by up to 200 Wm^{-2} while overestimates the LW radiation by up to 150 Wm^{-2} (maximum overestimations throughout the simulation period) due to the misrepresentation of the dust AODs. Even higher model overestimations of the SW radiation are observed at 12 UTC on 22 April 2007 attributed mainly to the inability of the model to reproduce satisfactorily clouds, since the negative model-AERONET differences of AOD cannot explain these large discrepancies in radiation. Clouds play an important role in such comparisons, particularly when their features are not well reproduced by the model, leading to large overestimations or underestimations, by up to 600 Wm^{-2} in absolute terms among the studied cases of the present analysis, as it has been pointed out in previous studies (e.g. Spyrou et al., 2013). Finally, the model (RADON) overestimation of the SW radiation reaching the ground, by up to 200 Wm^{-2} at 09 UTC on 21 April 2007, is probably associated with underestimation of the simulated dust AOD since fair weather conditions are forecasted and confirmed by the true color MODIS-Terra images (http://modis-atmos.gsfc.nasa.gov/IMAGES/). For the SW radiation, the positive NMMB-BSRN biases during the simulation period (21 April 2007 00 UTC – 24 April 2007 12 UTC) are reduced from 69.0 Wm^{-2} to 40.9 Wm^{-2} when dust-radiation interactions are activated (RADON) while lower positive biases for the LW radiation are calculated (0.7 Wm^{-2}) when dust-radiation interactions are deactivated (RADOFF). Summarizing, in the majority of the studied desert dust outbreaks here, positive and negative model-observations biases are found for the downwelling SW (Table S1) and LW (Table S2) radiation, respectively, which are reduced when the dust-radiation interactions are activated. On the contrary, similar improvements are not evident on the correlation coefficients since are not found remarkable differences between RADON-BSRN and RADOFF-BSRN R values (results not shown).

5.7. Assessment of the temperature fields versus analysis datasets

The forecasting performance of the NMMB-MONARCH model, except for the radiation (Section 5.6), has been also assessed for the temperature fields, utilizing as reference final analyses (FNL) derived from the National Centers for Environmental Prediction database (http://rda.ucar.edu/). The evaluation of both model configurations (RADON and RADOFF) against FNL temperature at 2 meters and at 17 pressure levels into the atmosphere is made at a regional scale for the NSD. For the former intercomparison, only land grid points are taken into account since the atmospheric driver is not coupled with an ocean model, while for the latter one it is not applied any criterion regarding the surface type (land or sea). The evaluation of the model is made by considering grid points where the dust AOD is higher/equal than 0.1, 0.5 and 1.0 representing low, moderate and intense dust load conditions, respectively. In order to overcome spatial inconsistencies between model and analyses, the model outputs have been regridded from their raw spatial resolution (0.25° x 0.25° degrees) to 1° x 1° degrees to match FNL. We note that analyses datasets are only "best" estimates of the observed states of the atmosphere and the surface produced by combining a model (in this case GFS) and available observations through data assimilation techniques. Analysis datasets are more poorly constrained by observations over certain regions including the arid and dusty ones, and more dependent on the model's behavior. This is even more relevant for surface variables such as 2-m temperature which may heavily depend on the underlying model's soil scheme.

In Figure 11, are presented the regional biases (model - FNL) of temperature at 2 meters for the RADON (red curve) and RADOFF (blue curve) experiments, averaged from the 20 desert dust outbreaks every 6 hours of the hindcast period, considering only land grid points where the dust AOD is higher/equal than: (i) 0.1, (ii) 0.5 and (iii) 1.0. Regardless of the dust AOD threshold, cold biases are found during night and early morning hours, warm biases are calculated in the afternoon while the minimum biases in absolute terms appear at noon. According to our results, under low desert dust conditions (Fig. 11-i), the agreement between model and FNL is better when the dust radiative effects are neglected (RADOFF) during daytime, while slightly lower RADON-FNL biases compared to RADOFF-FNL ones are found during night. At noon, the RADOFF-FNL biases are almost zero (less than 0.l K) whereas negative RADON-FNL biases (down to -0.27 K) are computed due to the surface cooling induced by the mineral particles. For moderate dust AODs (Fig. 11-ii), during night, the model-FNL temperature biases are lower for the RADON configuration (less than 1 K) in contrast to the RADOFF simulation (less than 1.4 K) and these improvements are statistically significant at 95%

confidence level. Nevertheless, at midday, the RADOFF-FNL biases are similar to those found for the lowest dust AOD threshold (Fig. 11-i), while the model cold biases, varying from -1.15 K (84 h) to -0.55 K (12 h), are amplified when the dust-radiation interactions are activated (RADON). The "corrections" of the near surface temperature forecasts during nighttime become more evident and statistically significant, when only land areas affected by intense dust loads (dust AOD ≥ 1.0) are considered in the NMMB-FNL comparison. Under these high dust AODs, the increase of air temperature at 2 meters due to the dust LW DREs reduces the existing cold biases. Therefore, the improvements on model's predictability of temperature at 2 meters when accounting for dust-radiation interactions, are more evident when the intensity of dust loads increases.

The potential impacts of the dust radiative effects inclusion on the model's forecasting ability have been also investigated for the temperature fields in vertical. For this purpose, from the 20 desert dust outbreaks, the temperature model-FNL biases at 17 pressure levels (from 1000 to 100 hPa) have been calculated in RADOFF (black curve) and RADON (red curve) and the obtained results are illustrated in Figure 12. The assessment results are presented only 24 (a) and 48 (b) hours after the initialization of the forecast period since are not found remarkable differences between the two model configurations at noon (i.e. 12 and 36 UTC).

Based on our findings, model warm biases are found between 950 and 700 hPa where most of the dust is confined (brown curve). For the lowest dust AOD threshold, these positive model-FNL biases reach up to 0.245 K and 0.313 K at 24 and 48 forecast hours, respectively, when mineral particles are not treated as radiatively active substance (RADOFF). On the contrary, when dust-radiation interactions are activated (RADON) the corresponding biases are reduced down to 0.155 K and 0.239 K, respectively, indicating a better model performance which is further supported by the fact that these improvements are statistical significant (95 % confidence level). Similar but more evident results are found when the dust AOD threshold increases from 0.1 to 0.5 (middle row in Figure 12). More specifically, at 24 forecast hours, the RADON-FNL temperature differences do not exceed 0.321 K in contrast to the corresponding biases between RADOFF and FNL which can be as high as 0.512 K. At 48 forecast hours, between altitudes where the dust concentrations are maximized, the red curve (RADON-FNL) is close to the blue thick line which represents the ideal score (i.e. zero biases), while the RADOFF warm biases can reach up to 0.443 K. As it has been shown in Section 5.4 (see Fig. 8 ii-b), due to the emission of longwave radiation by the mineral particles there is a temperature reduction within the atmospheric layers in which they are confined and a slight warming above the dust layer. The former effect explains the statistically significant reduction of the model warm biases between 950 and 700 hPa whereas the latter one could explain the slight statistically significant reduction of the model cold biases recorded between 600 and 500 hPa (see Fig. 12 ii-a). For the highest dust AOD threshold, at 24 forecast hours (Fig. 12 iii-a), the agreement of temperature profiles between RADON and FNL is better compared to RADOFF-FNL whereas at 48 forecast hours depends on altitude (Fig. 12 iii-b). Summarizing, thanks to the consideration of the dust radiative effects the predictive skills of the NMMB-MONARCH model in terms of reproducing temperature fields within the atmosphere are improved. Our findings are in agreement with previous studies in which similar evaluations have been made either against analyses datasets (Pérez et al., 2006) or weather station observations (Wang et al., 2010; Wang and Niu, 2013).

6. Summary and conclusions

In the present study, the direct radiative effects (DREs) induced by 20 intense and widespread Mediterranean desert dust outbreaks, that took place during the period March 2000 – February 2013, have been analyzed based on short-term (84 hours) regional simulations of the NMMB-MONARCH model. The identification of desert dust outbreaks has been accomplished via an objective and dynamic algorithm (Gkikas et al., 2013; 2016) utilizing as inputs daily satellite retrievals, available at 1° x 1° spatial resolution, providing information about aerosols' load (*AOD*), size (*FF*, α) and nature (*AI*). DREs have been calculated at the top of the atmosphere (TOA), into the atmosphere (ATM), and at the surface, for the downwelling (SURF) and the absorbed (NETSURF) radiation, for the shortwave (SW), longwave (LW) and NET (SW+LW) radiation. The obtained results have been presented through geographical distributions as well as at regional level by averaging the clear-sky DREs over the whole simulation domain (NSD), the Sahara Desert (SDD) and the broader Mediterranean basin (MSD) sub-domains. At a further step, the impacts of desert dust outbreaks on sensible and latent heat fluxes as well as on temperature at 2 meters and into the atmosphere have been investigated. Moreover, the potential feedbacks on dust emission and dust AOD, attributed to dust-radiation interactions, have been assessed at regional scale representative for the simulation domain used in our experiments. In the last part of our study, focus was given on the potential improvements on model's predictive skills, attributed to the inclusion of dust radiative effects into the numerical simulations, in terms of reproducing the downward SW/LW radiation at the ground as well as the temperature fields. The main findings obtained from the present analysis are summarized below.

Direct Radiative Effects

- DREs into the atmosphere and at the surface are driven by the dust outbreaks' spatial features whereas at TOA, the surface albedo plays a crucial role, particularly under clear sky conditions.
- At noon, dust outbreaks induce a strong surface cooling with instantaneous NET DRE_{SURF} values down to -589 Wm^{-2}.
- Similar spatial patterns are revealed for the absorbed radiation at the ground; however, the magnitude of the NET $DRE_{NETSURF}$ values is lower in comparison with the corresponding DREs for SURF.
- Through the absorption of the incoming solar radiation by the mineral particles, dust outbreaks can increase the atmospheric radiation budget (warming effect) by up to 319 Wm^{-2} around midday.
- At TOA, positive DREs up to 85 Wm^{-2} are found over highly reflective surfaces indicating a planetary warming while negative DREs down to -184 Wm^{-2} are computed over dark surfaces indicating a strong planetary cooling.
- During nighttime, reverse effects of lower magnitude are found into the atmosphere and at the surface with maximum instantaneous NET DRE_{SURF}, $DRE_{NETSURF}$ and DRE_{ATM} values equal to 83 Wm^{-2}, 50 Wm^{-2} and -61 Wm^{-2} whereas at TOA due to the offset of the atmospheric cooling by the surface warming, the DRE_{TOA} values are almost negligible (less than 10 Wm^{-2}).
- The regional NET clear-sky DREs for the NSD range from -13.9 to 2.6 Wm^{-2}, from -43.6 to 4 Wm^{-2}, from -26.3 to 3.9 Wm^{-2} and from -3.7 to 28 Wm^{-2} for TOA, SURF, NETSURF and ATM, respectively.
- For the regional clear-sky NET DREs at TOA, the calculated positive DREs (7.1 Wm^{-2}) in the SDD and the negative DREs (-15 Wm^{-2}) in the MSD at noon indicate a planetary warming and cooling in the Sahara and in the Mediterranean, respectively.
- Over the 84 hours forecast period, the LW surface warming offsets by up to 37.7% the SW surface cooling whereas the LW atmospheric cooling offsets by 33.6% the SW atmospheric warming.
- At TOA, the corresponding LW/SW ratios vary from 15.4% (MSD) to 52.9% (SDD); however, the contribution of the LW DREs to the NET ones is comparable or even larger, particularly over the Sahara at midday.

Atmos. Chem. Phys. Discuss., https://doi.org/10.5194/acp-2017-932
Manuscript under review for journal Atmos. Chem. Phys.
Discussion started: 10 November 2017

Atmospheric Chemistry and Physics Discussions

Sensible and latent heat fluxes

- As a response to the surface radiation budget perturbations, desert dust outbreaks reduce the sensible heat fluxes (regional averages taking into account only land grid points) by up to 45 Wm^{-2} during daytime while reverse tendencies of lower magnitudes are found during night (2 Wm^{-2}).
- Locally, the aforementioned values can reach down to -150 Wm^{-2} and up to 50 Wm^{-2}.
- At noon, dust outbreaks reduce also the surface latent heat fluxes by up to 4 Wm^{-2} and 100 Wm^{-2} at a regional and grid point level, respectively. At night, the regional and the instantaneous LE levels are increased by up to 0.5 Wm^{-2} and 30 Wm^{-2}, respectively.

Impact on temperature fields

- Due to the attenuation of the incoming solar radiation and the emission of radiation at thermal wavelengths, both induced by dust aerosols, temperature at 2 meters reduces and increases during day and night, respectively, by up to 4 K in absolute terms in land areas where the dust loads are maximized (AODs higher than 2).
- At noon, dust outbreaks warm the atmosphere by up to 0.9 K between altitudes where elevated dust layers are located and cool the lowest tropospheric levels by up to 1.3 K, due to the reduced surface sensible heat fluxes.
- Due to the emission of LW radiation and the trapping of the outgoing terrestrial radiation by dust aerosols, the nocturnal temperature decreases by up to 0.8 K in atmospheric altitudes where mineral particles are confined, whereas between the bottom of the dust layer and the surface, the air-temperature increases by up to 1.2 K.

Feedbacks on dust AOD and dust emission

- The total emitted amount of dust is reduced by 19.5% (statistically significant at 95% confidence level) over the forecast period when dust DREs are included into the numerical simulations, revealing thus a negative feedback on dust emissions.
- Among the studied cases, the corresponding percentages range from -34% (2 August 2012) to -10% (24 February 2006) and are statistical significant (95% confidence level) in all cases.

- As a consequence of the lower amount of mineral particles emitted in the atmosphere, negative feedbacks are also found on the mean regional dust AOD_{550nm} which is decreased by 0.02 (6.9%) with respect to the control experiment (RADOFF).
- Statistically significant reductions of the regional dust AOD_{550nm}, varying from 1% (22 February 2004) to 12.5% (27 January 2005), are found in all the studied cases when dust-radiation interactions are activated (RADON).

Assessment of model's predictive skills

- Through the evaluation of the model's forecast outputs of the downwelling SW and LW radiation at the ground against surface measurements derived by the BSRN network, it is revealed a reduction of the modelled positive and negative biases for the SW and LW radiation, respectively, attributed to the consideration of the dust radiative effects. However, model's accuracy is critically affected by its ability to represent satisfactorily clouds' spatiotemporal features highlighting thus the key role of other model errors when such comparisons are attempted.
- Under high dust load conditions (AODs higher/equal than 0.5), the nocturnal model-FNL negative regional biases of temperature at 2 meters are reduced by up to 0.5 K (95% statistically significant) in the RADON experiment. On the contrary, these temperature "corrections" are not evident during daytime revealing thus that other model errors (particularly those introduced by the soil model) can dominate over the expected improvements attributed to the consideration of dust-radiation interactions in the numerical simulations.
- The model regional warm biases found at 24 and 48 hours after the initialization of the forecast period, between pressure levels (950 and 700 hPa) where the dust concentration is maximized, are reduced by up to 0.4 K (95% statistically significant) in the RADON experiment.

Acknowledgments

The MDRAF project has received funding from the European Union's Seventh Framework Programme for research, technological development and demonstration under grant agreement no 622662. O. Jorba and S. Basart acknowledge the grant CGL2013-46736 and the AXA Research Fund. C. Pérez García-Pando acknowledges long-term support from the AXA Research Fund, as well as the support received through the Ramón y Cajal programme (grant RYC-2015-18690) of the Spanish Ministry of Economy and Competitiveness. Simulations were performed with the Marenostrum Supercomputer at the

Barcelona Supercomputing Center (BSC). We would like to thank the principal investigators maintaining the BSRN sites used in the present work. The authors would like thank the Arnon Karnieli for his effort in establishing and maintaining SEDE_BOKER AERONET site.

References

Ahn, H. J., Park, S. U., and Chang, L. S.: Effect of direct radiative forcing of Asian dust on the meteorological fields in East Asia during an Asian dust event period, J. Appl. Meteorol., 46, 1655–1681, doi:10.1175/JAM2551.1, 2007.

Albrecht, B. A.: Aerosols, cloud microphysics, and fractional cloudiness, *Science*, 245, 1227–1230, 1989.

Alpert, P. and Ziv, B.: The Sharav Cyclone: Observations and some theoretical considerations, J. Geophys. Res., 94, 18495–18514, doi:10.1029/JD094iD15p18495, 1989.

Amiridis, V., Kafatos, M., Perez, C., Kazadzis, S., Gerasopoulos, E., Mamouri, R. E., Papayannis, A., Kokkalis, P., Giannakaki, E., Basart, S., Daglis, I., and Zerefos, C.: The potential of the synergistic use of passive and active remote sensing measurements for the validation of a regional dust model, Ann. Geophys., 27, 3155-3164, doi:10.5194/angeo-27-3155-2009, 2009.

Antón, M., Valenzuela, A., Cazorla, A., Gil, J. E., Fernández-Gálvez, J., Lyamani, H., Foyo-Moreno, I., Olmo, F. J., and Alados-Arboledas, L.: Global and diffuse shortwave irradiance during a strong desert dust episode at Granada (Spain), Atmos. Res., 118, 232–239, doi:10.1016/j.atmosres.2012.07.007, 2012.

Antón, M., Valenzuela, A., Mateos, D., Alados, I., Foyo-Moreno, I., Olmo, F.J., Alados-Arboledas, L.: Longwave aerosol radiative effects during an extreme desert dust event in Southeastern Spain, Atmos. Res., 148, 18–23, doi:10.1016/j.atmosres.2014.05.022, 2014.

Arakawa, A. and Lamb, V. R.: Computational design of the basic dynamical processes of the UCLA general circulation model, Meth. Comput. Phys., 17, 173–265, 1977.

Atmos. Chem. Phys. Discuss., https://doi.org/10.5194/acp-2017-932
Manuscript under review for journal Atmos. Chem. Phys.
Discussion started: 10 November 2017

Badia, A., Jorba, O., Voulgarakis, A., Dabdub, D., Pérez García-Pando, C., Hilboll, A., Gonçalves, M., and Janjic, Z.: Description and evaluation of the Multiscale Online Nonhydrostatic AtmospheRe CHemistry model (NMMB-MONARCH) version 1.0: gas-phase chemistry at global scale, Geosci. Model Dev., 10, 609-638, doi:10.5194/gmd-10-609-2017, 2017.

Banks, J. R., Brindley, H. E., Hobby, M., and Marsham, J. H.: The daytime cycle in dust aerosol direct radiative effects observed in the central Sahara during the Fennec campaign in June 2011, J. Geophys. Res.-Atmos., 119, 13861–13876, doi:10.1002/2014JD022077, 2014.

Barkan, J., Alpert, P., Kutiel, H., and Kishcha, P.: Synoptics of dust transportation days from Africa toward Italy and central Europe, J. Geophys. Res., 110, D07208, doi:10.1029/2004JD005222, 2005.

Basart, S., Pérez, C., Cuevas, E., Baldasano, J. M., and Gobbi, G. P.: Aerosol characterization in Northern Africa, Northeastern Atlantic, Mediterranean Basin and Middle East from direct-sun AERONET observations, Atmos. Chem. Phys., 9, 8265-8282, https://doi.org/10.5194/acp-9-8265-2009, 2009.

Bergstrom, R. W., Pilewskie, P., Russell, P. B., Redemann, J., Bond, T. C., Quinn, P. K., and Sierau, B.: Spectral absorption properties of atmospheric aerosols, Atmos. Chem. Phys., 7, 5937-5943, doi:10.5194/acp-7-5937-2007, 2007.

Betts, A. K.: A new convective adjustment scheme. Part 1: Observational and theoretical basis, Q. J. Roy. Meteor. Soc., 112, 677–691, doi:10.1002/qj.49711247307, 1986.

Betts, A. K. and Miller, M. J.: A new convective adjustment scheme. Part 2: Single column tests using GATE wave, BOMEX, ATEX and arctic air-mass data sets, Q. J. Roy. Meteor. Soc., 112, 693–709, doi:10.1002/qj.49711247308, 1986.

Binietoglou, I., Basart, S., Alados-Arboledas, L., Amiridis, V., Argyrouli, A., Baars, H., Baldasano, J. M., Balis, D., Belegante, L., Bravo-Aranda, J. A., Burlizzi, P., Carrasco, V., Chaikovsky, A., Comerón, A., D'Amico, G., Filioglou, M., Granados-Muñoz, M. J., Guerrero-Rascado, J. L., Ilic, L., Kokkalis, P., Maurizi, A., Mona, L., Monti, F., Muñoz-Porcar, C., Nicolae, D., Papayannis, A., Pappalardo, G., Pejanovic, G., Pereira, S. N., Perrone, M. R., Pietruczuk, A., Posyniak, M., Rocadenbosch, F., Rodríguez-Gómez, A., Sicard, M., Siomos, N., Szkop, A., Terradellas, E., Tsekeri, A., Vukovic, A., Wandinger, U.,

Atmos. Chem. Phys. Discuss., https://doi.org/10.5194/acp-2017-932
Manuscript under review for journal Atmos. Chem. Phys.
Discussion started: 10 November 2017

and Wagner, J.: A methodology for investigating dust model performance using synergistic EARLINET/AERONET dust concentration retrievals, Atmos. Meas. Tech., 8, 3577-3600, doi:10.5194/amt-8-3577-2015, 2015.

Boucher, O., Randall, D., Artaxo, P., Bretherton, C., Feingold, G., Forster, P., Kerminen, V.-M., Kondo, Y., Liao, H., Lohmann, U., Rasch, P., Satheesh, S.K., Sherwood, S., Stevens B., and Zhang, X.Y.: Clouds and Aerosols. In: *Climate Change 2013: The Physical Science Basis. Contribution of Working Group I to the Fifth Assessment Report of the Intergovernmental Panel on Climate Change* [Stocker, T.F., D. Qin, G.-K. Plattner, M. Tignor, S.K. Allen, J. Boschung, A. Nauels, Y. Xia, V. Bex and P.M. Midgley (eds.)]. Cambridge University Press, Cambridge, United Kingdom and New York, NY, USA, pp. 571–658, doi:10.1017/CBO9781107415324.016, 2013.

Carnevale, C., Finzi, G., Pisoni, E., Volta, M., Kishcha, P., and Alpert, P.: Integrating Saharan dust forecasts into a regional chemical transport model: a case study over Northern Italy, Sci.Total Environ., 417–418, 224–231, 2012.

Chin, M., Ginoux, P., Kinne, S., Torres, O., Holben, B. N., Duncan, B. N., Martin, R. V., Logan, J. A., Higurashi, A., and Nakajima, T.: Tropospheric aerosol optical thickness from the GOCART model and comparisons with satellite and Sun photometer measurements, J. Atmos. Sci., 59, 461–483, doi:10.1175/1520-0469(2002)059<0461:TAOTFT>2.0.CO, 2002.

Choobari, O. A., Zawar-Reza, P., Sturman, A.: Feedback between windblown dust and planetary boundary-layer characteristics: sensitivity to boundary and surface layer parameterizations. Atmos. Environ., 61, 294–304, http://dx.doi.org/10.1016/j.atmosenv.2012.07.038, 2012.

Choobari, O. A., Zawar-Reza, P., and Sturman, A.: The global distribution of mineral dust and its impacts on the climate system: A review, Atmos. Res., 138, 152-165, doi:10.1016/j.atmosres.2013.11.007, 2014.

Christopher, S. A. and Jones, T. A.: Satellite-based assessment of cloud-free net radiative effect of dust aerosols over the Atlantic Ocean, Geophys. Res. Lett., 34, L02810, doi:10.1029/2006GL027783, 2007.

Colarco, P. R., Nowottnick, E. P., Randles, C. A., Yi, B., Yang, P., Kim, K.-M., Smith, J. A., and Bardeen, C. G.: Impact of radiatively interactive dust aerosols in the NASA GEOS-5 climate model: Sensitivity to dust particle shape and refractive index, J. Geophys. Res.-Atmos., 119, 753–786, doi:10.1002/2013JD020046, 2014.

Cowie, S. M., Knippertz, P., and Marsham, J. H.: A climatology of dust emission events from northern Africa using long-term surface observations, Atmos. Chem. Phys., 14, 8579-8597, doi:10.5194/acp-14-8579-2014, 2014.

Cuesta, J., Marsham, J. H., Parker, D. J., and Flamant, C.: Dynamical mechanisms controlling the vertical redistribution of dust and the thermodynamic structure of the West Saharan atmospheric boundary layer during summer, Atmos. Sci. Lett., 10, 34–42, doi:10.1002/Asl.207, 2009.

DeSouza-Machado, S. G., Strow, L. L., Imbiriba, B., McCann, K., Hoff, R. M., Hannon, S. E., Martins, J. V., Tanré, D., Deuzé, J. L., Ducos, F., and Torres, O.: Infrared retrievals of dust using AIRS: Comparisons of optical depths and heights derived for a North African dust storm to other collocated EOS ATrain and surface observations, J. Geophys. Res., 115, D15201, doi:10.1029/2009JD012842, 2010.

Di Biagio, C., di Sarra, A., and Meloni, D.: Large atmospheric shortwave radiative forcing by Mediterranean aerosol derived from simulteneous ground-based and spaceborne observations, and dependence on the aerosol type and single scattering albedo, J. Geophys. Res., 115, D10209, doi:10.1029/2009JD012697, 2010.

Di Sarra, A., Pace, G., Meloni, D., De Silvestri, L., Piacentino, S., and Monteleone, F.: Surface shortwave radiative forcing of different aerosol types in the central Mediterranean, Geophys. Res. Lett., 35, L02714, doi:10.1029/2007GL032395, 2008.

Di Sarra, A., di Biagio, C., Meloni, D., Monteleone, F., Pace, G., Pugnaghi, S., and Sferlazzo, D.: Shortwave and longwave radiative effects of the intense Saharan dust event of 25–26 March 2010 at Lampedusa (Mediterranean Sea), J. Geophys. Res., 116, D23209, doi:10.1029/2011JD016238, 2011.

Di Sarra, A., Fuà, D., and Meloni, D.: Estimate of surface direct radiative forcing of desert dust from atmospheric modulation of the aerosol optical depth, Atmos. Chem. Phys., 13, 5647-5654, doi:10.5194/acp-13-5647-2013, 2013.

Di Tomaso, E., Schutgens, N. A. J., Jorba, O., and Pérez García-Pando, C.: Assimilation of MODIS Dark Target and Deep Blue observations in the dust aerosol component of NMMB-MONARCH version 1.0, Geosci. Model Dev., 10, 1107-1129, doi:10.5194/gmd-10-1107-2017, 2017.

Ek, M. B., Mitchell, K. E., Lin, Y., Rogers, E., Grunmann, P., Koren, V., Gayno, G., and Tarpley, J. D.: Implementation of Noah land surface model advances in the National Centers for Environmental Prediction operational mesoscale Eta model, J. Geophys. Res., 108, 8851, doi:10.1029/2002JD003296, 2003.

Ferrier, B. S., Jin, Y., Lin, Y., Black, T., Rogers, E., and DiMego, G.: Implementation of a new grid-scale cloud and precipitation scheme in the NCEP Eta Model, in: Proc. 15th Conf. on Numerical Weather Prediction, 12–16 August 2002, San Antonio, TX, Amer. Meteor. Soc., pp. 280–283, 2002.

Foltz, G. R. and McPhaden, M. J.: Impact of Saharan dust on tropical North Atlantic SST, J. Climate, 21, 5048–5060, 2008.

Gama, C., Tchepel, O., Baldasano, J. M., Basart, S., Ferreira, J., Pio, C., Cardoso, J., and Borrego, C.: Seasonal patterns of Saharan dust over Cape Verde-a combined ap- proach using observations and modelling, Tellus B, 67, 24410, doi:10.3402/tellusb.v67.24410, 2015.

Ginoux, P., Prospero, J. M., Gill, T. E., Hsu, N. C., and Zhao, M.: Global-scale attribution of anthropogenic and natural dust sources and their emission rates based on MODIS Deep Blue aerosol products, Rev. Geophys., 50, RG3005, doi:10.1029/2012rg000388, 2012.

Gkikas, A., Hatzianastassiou, N., Mihalopoulos, N., Katsoulis, V., Kazadzis, S., Pey, J., Querol, X., and Torres, O.: The regime of intense desert dust episodes in the Mediterranean based on contemporary satellite observations and ground measurements, Atmos. Chem. Phys., 13, 12135-12154, doi:10.5194/acp-13-12135-2013, 2013.

Gkikas, A., Houssos, E. E., Lolis, C. J., Bartzokas, A., Mihalopoulos, N. and Hatzianastassiou, N.: Atmospheric circulation evolution related to desert-dust episodes over the Mediterranean. Q.J.R. Meteorol. Soc., 141: 1634–1645. doi: 10.1002/qj.2466, 2015.

Gkikas, A., Basart, S., Hatzianastassiou, N., Marinou, E., Amiridis, V., Kazadzis, S., Pey, J., Querol, X., Jorba, O., Gassó, S., and Baldasano, J. M.: Mediterranean intense desert dust outbreaks and their vertical

Atmos. Chem. Phys. Discuss., https://doi.org/10.5194/acp-2017-932
Manuscript under review for journal Atmos. Chem. Phys.
Discussion started: 10 November 2017

Atmospheric Chemistry and Physics Discussions

structure based on remote sensing data, Atmos. Chem. Phys., 16, 8609-8642, doi:10.5194/acp-16-8609-2016, 2016.

Gómez-Amo, J. L., Pinti, V., Di Iorio, T., di Sarra, A., Meloni, D., Becagli, S., Bellantone, V., Cacciani, M., Fuà, D., and Perrone, M. R.: The June 2007 Saharan dust event in the central Mediterranean: Observations and radiative effects in marine, urban, and sub-urban environments, Atmos. Environ., 45, 5385–5493, 2011.

Guerrero-Rascado, J. L., Olmo, F. J., Avilés-Rodríguez, I., Navas-Guzmán, F., Pérez-Ramírez, D., Lyamani, H., and Alados Arboledas, L.: Extreme Saharan dust event over the southern Iberian Peninsula in september 2007: active and passive remote sensing from surface and satellite, Atmos. Chem. Phys., 9, 8453-8469, doi:10.5194/acp-9-8453-2009, 2009.

Hansen, J., Sato, M., and Ruedy, R.: Radiative forcing and climate response, J. Geophys. Res., 102, 6831–6864, 1997.

Hatzianastassiou, N., Katsoulis, B., and Vardavas, I.: Sensitivity analysis of aerosol direct radiative forcings in the ultraviolet – visible wavelengths and consequences for the heat budget, Tellus, 56B, 368–381, 2004.

Haustein, K., Pérez, C., Baldasano, J. M., Jorba, O., Basart, S., Miller, R. L., Janjic, Z., Black, T., Nickovic, S., Todd, M. C., Washington, R., Müller, D., Tesche, M., Weinzierl, B., Esselborn, M., and Schladitz, A.: Atmospheric dust modeling from meso to global scales with the online NMMB/BSC-Dust model – Part 2: Experimental campaigns in Northern Africa, Atmos. Chem. Phys., 12, 2933-2958, doi:10.5194/acp-12-2933-2012, 2012.

Haywood, J., Allan, R., Culverwell, I., Slingo, T., Milton, S., Edwards, J., and Clerbaux, N.: Can desert dust explain the outgoing longwave radiation anomaly over the Sahara during July 2003? J. Geophys. Res., 110, D05105, doi:10.1029/2004JD005232, 2005.

Atmos. Chem. Phys. Discuss., https://doi.org/10.5194/acp-2017-932
Manuscript under review for journal Atmos. Chem. Phys.
Discussion started: 10 November 2017

Heald, C. L., Ridley, D. A., Kroll, J. H., Barrett, S. R. H., Cady-Pereira, K. E., Alvarado, M. J., and Holmes, C. D.: Contrasting the direct radiative effect and direct radiative forcing of aerosols, Atmos. Chem. Phys., 14, 5513-5527, doi:10.5194/acp-14-5513-2014, 2014.

Heinold, B., Tegen, I., Schepanski, K., and Hellmuth, O.: Dust Radiative feedback on Saharan boundary layer dynamics and dust mobilization. Geophys. Res. Lett.,35, L20817, doi:10.1029/2008GL035319, 2008.

Helmert, J., Heinold, B., Tegen, I., Hellmuth, O., and Wendisch, M.: On the direct and semidirect effect of Saharan dust over Europe: a modeling study, J. Geophys. Res., 112, D11204, doi:10.1029/2006JD007444, 2007.

Huang, J., Wang, T., Wang, W., Li, Z., and Yan, H.: Climate effects of dust aerosols over East Asian arid and semi-arid regions, J. Geophys. Res., 119, 11398–11416, doi:10.1002/2014JD021796, 2014.

Huneeus, N., Basart, S., Fiedler, S., Morcrette, J.-J., Benedetti, A., Mulcahy, J., Terradellas, E., Pérez García-Pando, C., Pejanovic, G., Nickovic, S., Arsenovic, P., Schulz, M., Cuevas, E., Baldasano, J. M., Pey, J., Remy, S., and Cvetkovic, B.: Forecasting the northern African dust outbreak towards Europe in April 2011: a model intercomparison, Atmos. Chem. Phys., 16, 4967-4986, doi:10.5194/acp-16-4967-2016, 2016.

Iacono, M. J., Delamere, J. S., Mlawer, E. J., Shephard, M. W., Clough, S. A., and Collins, W. D.: Radiative forcing by long-lived greenhouse gases: Calculations with the AER Radiative transfer models, J. Geophys. Res., 113, D13103, doi:10.1029/2008JD009944, 2008.

IPCC, 2013: *Climate Change 2013: The Physical Science Basis. Contribution of Working Group I to the Fifth Assessment Report of the Intergovernmental Panel on Climate Change* [Stocker, T.F., D. Qin, G.-K. Plattner, M. Tignor, S.K. Allen, J. Boschung, A. Nauels, Y. Xia, V. Bex and P.M. Midgley (eds.)]. Cambridge University Press, Cambridge, United Kingdom and New York, NY, USA, 1535 pp, doi:10.1017/CBO9781107415324.

Atmos. Chem. Phys. Discuss., https://doi.org/10.5194/acp-2017-932
Manuscript under review for journal Atmos. Chem. Phys.
Discussion started: 10 November 2017

Janjic, Z. I.: The step-mountain eta coordinate model: further developments of the convection, viscous sublayer, and tur- bulence closure schemes, Mon. Weather Rev., 122, 927–945, doi:10.1175/1520-0493(1994)122<0927:TSMECM>2.0.CO;2, 1994.

Janjic, Z. I.: Comments on “Development and evalua- tion of a convection scheme for use in climate mod- els”, J. Atmos. Sci., 57, 3686–3686, doi:10.1175/1520-0469(2000)057<3686:CODAEO>2.0.CO;2, 2000.

Janjic, Z. I., Gerrity, J. P., and Nickovic, S.: An alternative approach to nonhydrostatic modeling, Mon. Weather Rev., 129, 1164–1178, doi:10.1175/1520- 0493(2001)1292.0.CO;2, 2001.

Janjic, Z. I.: A nonhydrostatic model based on a new approach, Meteorol. Atmos. Phys., 82, 271–285, doi:10.1007/s00703-001- 0587-6, 2003.

Janjic, Z. I.: A unified model approach from meso to global scales, Geophys. Res. Abstr., 7, SRef–ID: 1607–7962/gra/EGU05–A– 05582, 2005.

Janjic, Z. I. and Black, T.: A unified model approach from meso to global scales, Geophys. Res. Abstr., 9, SRef–ID: 1607–7962/gra/EGU2007–A–05025, 2007.

Janjic, Z.: Further development of the unified multiscale Eulerian model for a broad range of spatial and temporal scales within the new National Environmental Modeling System, EGU General Assembly 2009, held 19–24 April 2009, Vienna, Austria, abstract #EGU2009-1587, 11, p. 1587, 2009.

Janjic, Z., Janjic, T., and Vasic, R.: A Class of conservative fourth order advection schemes and impact of enhanced formal accuracy on extended range forecasts, Mon. Weather Rev., 0, null, doi:10.1175/2010MWR3448.1, 2011.

Ji, Z., Wang, G., Pal, J.S., Yu, M.: Potential climate effect of mineral aerosols over West Africa. Part I: model validation and contemporary climate evaluation. Clim. Dyn.,1–17, doi: 10.1007/s00382-015-2641-y, 2015.

Kalenderski, S. and Stenchikov, G.: High-resolution regional modeling of summertime transport and impact of African dust over the Red Sea and Arabian Peninsula, J. Geophys. Res., 121, 6435-6458, doi: 10.1002/2015JD024480, 2016.

Kanakidou, M., Mihalopoulos, N., Kalivitis, N., Tsigaridis, K., Kouvarakis, G., Koulouri, E., Gerasopoulos, E., Vrekoussis, M., and Myriokefalitakis, S.: Natural contributions to particulate matter levels over Europe – the experience from Greece, International Conference on Science and Technology (CEST) 2007, A-585-592, 2007.

Kubilay, N., Cokacar, T., and Oguz, T.: Optical properties of mineral dust outbreaks over the northeastern Mediterranean, J. Geophys. Res., 108(D21), 4666, doi:10.1029/2003JD003798, 2003.

Kumar, R., Barth, M. C., Pfister, G. G., Naja, M., and Brasseur, G. P.: WRF-Chem simulations of a typical pre-monsoon dust storm in northern India: influences on aerosol optical properties and radiation budget, Atmos. Chem. Phys., 14, 2431–2446, doi:10.5194/acp-14-2431-2014, 2014.

Lelieveld, J., Berresheim, H., Borrmann, S., et al.: Global air pollution crossroads over the Mediterranean, *Science*, 298, 794–799, 2002.

Liao, H. and Seinfeld, J.: Radiative forcing by mineral dust aerosols: sensitivity to key variables, J. Geophys. Res., 103, 31637–31645, 1998.

Ling, X., Guo, W., and Fu, C.: Composite analysis of impacts of dust aerosols on surface atmospheric variables and energy budgets in a semiarid region of China, J. Geophys. Res. Atmos., 119, 3107–3123, doi:10.1002/2013jd020274, 2014.

Lohmann, U. and Feichter, J.: Global indirect aerosol effects: a review, Atmos. Chem. Phys., 5, 715-737, doi:10.5194/acp-5-715-2005, 2005.

Mahowald, N. M., Albani, S., Kok, J. F., Engelstaedter, S., Scanza, R., Ward, D. S., and Flanner, M. G.: The size distribution of desert dust aerosols and its impact on the Earth system, Aeol. Res., 15, 53–71, doi:10.1016/j.aeolia.2013.09.002, 2014.

Mallet, M., Tulet, P., Serça, D., Solmon, F., Dubovik, O., Pelon, J., Pont, V., and Thouron, O.: Impact of dust aerosols on the radiative budget, surface heat fluxes, heating rate profiles and convective activity over West Africa during March 2006, Atmos. Chem. Phys., 9, 7143-7160, doi:10.5194/acp-9-7143-2009, 2009.

Marcella, M.P., Eltahir, E.A.B.: The role of mineral aerosols in shaping the regional climate of West Africa. J. Geophys. Res., Atmospheres, 119, 1-14, doi:10.1002/2012JD019394, 2014.

Marti, A., Folch, A., Jorba, O., and Janjic, Z.: Volcanic ash modeling with the online NMMB-MONARCH-ASH v1.0 model: model description, case simulation, and evaluation, Atmos. Chem. Phys., 17, 4005-4030, doi:10.5194/acp-17-4005-2017, 2017.

McPeters, R.D., Bhartia, P. K., Krueger, A. J., Torres, O. and Herman, J. R.: Earth Probe Total Ozone Mapping Spectrometer (TOMS) Data Products User's Guide; NASA Technical Publication 1998-206895, 1998.

Meloni, D., di Sarra, A., Di Iorio, T., and Fiocco, G.: Direct radiative forcing of Saharan dust in the Mediterranean from measurements at Lampedusa island and MISR space-borne observations, J. Geophys. Res., 109(D8), D08206, doi:10.1029/2003JD003960, 2004.

Meloni, D., di Sarra, A., Monteleone, F., Pace, G., Piacentino, S., and Sferlazzo, D.: Seasonal transport patterns of intense Saharan dust events at the Mediterranean island of Lampedusa, Atmos. Res., 88, 134–148, doi:10.1016/j.atmosres.2007.10.007, 2008.

Meloni, D., Junkermann, W., di Sarra, A., Cacciani, M., De Silvestri, L., Di Iorio, T., Estellés, V., Gómez-Amo, J. L., Pace, G., and Sferlazzo, D. M.: Altitude-resolved shortwave and longwave radiative effects of desert dust in the Mediterranean during the GAMARF campaign: Indications of a net daily cooling in the dust layer, J. Geophys. Res., 120, 3386–3407, doi:10.1002/2014JD022312, 2015.

Meyer, K., Platnick, S., Oreopoulos, L., and Lee, D.: Estimating the direct radiative effect of absorbing aerosols overlying marine boundary layer clouds in the southeast Atlantic using MODIS and CALIOP, J. Geophys. Res.-Atmos., 118, 4801– 4815, doi:10.1002/jgrd.50449, 2013.

Miller, R. L. and Tegen, I.: Climate response to soil dust aerosols, J. Climate, 11, 3247–3267, 1998.

Miller, R. L., Perlwitz, J., and Tegen, I.: Feedback upon dust emission by dust radiative forcing through the planetary boundary layer, J. Geophys. Res., 109, D24209, doi:10.1029/2004JD004912, 2004a.

Miller, R. L., Tegen, I., and Perlwitz, J.: Surface radiative forcing by soil dust aerosols and the hydrologic cycle, J. Geophys. Res., 109(D4), D04203, doi:10.1029/2003JD004085, 2004b.

Mischenko, M., Travis, L. D., and Lacis, A. A.: Scattering, absorption and emission of light by small particles, Cambridge University Press, Cambridge, 2002.

Mishra, A.K., Koren, I., Rudich, Y.: Effect of aerosol vertical distribution on aerosol-radiation interaction: a theoretical prospect. Heliyon 1, e00036. http://dx.doi.org/10.1016/j.heliyon.2015.e00036, 2015.

Mlawer, E. J., Taubman, S. J., Brown, P. D., Iacono, M. J., and Clough, S. A.: Radiative transfer for inhomogeneous atmospheres: RRTM, a validated correlated-k model for the longwave, J. Geophys. Res., 102, 16663–16682, doi:10.1029/97JD00237, 1997.

Monin, A. S. and Obukhov, A. M.: Osnovnye zakonomernosti turbulentnogo peremesivanija v prizemnom sloe atmosfery, Trudy geofiz. inst. AN SSSR, 24, 163–187, 1954.

Moulin, C., Lambert, C. E., Dayan, U., Masson, V., Ramonet, M., Bousquet, P., Legrand, M., Balkanski, Y. J., Guelle, W., Marti- corena, B., Bergametti, G., and Dulac, F.: Satellite climatology of African dust transport in the Mediterranean atmosphere, J. Geo- phys. Res., 103, 13137, doi:10.1029/98JD00171, 1998.

Müller, T., Schladitz, A., Massling, A., Kaaden, N., Kandler, K., and Wiedensohler, A.: Spectral absorption coefficients and imaginary parts of refractive indices of Saharan dust during SAMUM-1, Tellus B, 61, 79–95, 2009.

Nabat, P., Solmon, F., Mallet, M., Kok, J. F., and Somot, S.: Dust emission size distribution impact on aerosol budget and radiative forcing over the Mediterranean region: a regional climate model approach, Atmos. Chem. Phys., 12, 10545-10567, doi:10.5194/acp-12-10545-2012, 2012.

Nabat, P., Somot, S., Mallet, M., Sevault, F., Chiacchio, M., and Wild, M.: Direct and semi-direct aerosol radiative effect on the Mediterranean climate variability using a Regional Climate System Model, Clim. Dynam., 44, 1127–1155, doi:10.1007/s00382-014-2205-6, 2015a.

Nabat, P., Somot, S., Mallet, M., Michou, M., Sevault, F., Driouech, F., Meloni, D., di Sarra, A., Di Biagio, C., Formenti, P., Sicard, M., Léon, J.-F., and Bouin, M.-N.: Dust aerosol radiative effects during summer 2012 simulated with a coupled regional aerosol–atmosphere–ocean model over the Mediterranean, Atmos. Chem. Phys., 15, 3303-3326, doi:10.5194/acp-15-3303-2015, 2015b.

Nastos, P. T.: Meteorological Patterns Associated with Intense Saharan Dust Outbreaks over Greece in Winter, Adv. Meteorol., 2012, 828301, 17 pp., 2012.

Obregón, M.A., Pereira, S., Salgueiro, V., Costa, M.J., Silva, A.M., Serrano, A., Bortoli, D.: Aerosol radiative effects during two desert dust events in August 2012 over the Southwestern Iberian Peninsula, Atmos. Res., 153, 404-415, doi:10.1016/j.atmosres.2014.10.007, 2015.

Ohmura, A., Gilgen, H., Hegner, H., Müller, G., Wild, M., Dutton, E. G., Forgan, B., Fröhlich, C., Philipona, R., Heimo, A., and König-Langlo, G.: Baseline Surface Radiation Network (BSRN/WCRP): New precision radiometry for climate research, B. Am. Meteorol. Soc., 79, 2115–2136, 1998.

O'Neill, N. T., Eck, T. F., Smirnov, A., Holben, B. N., and Thulasiraman, S.: Spectral discrimination of coarse and fine mode optical depth, J. Geophys. Res., 108, 4559, doi:10.1029/2002JD002975, 2003.

Oreopoulos, L., and Barker, H. W.: Accounting for subgrid-scale cloud variability in a multi-layer 1-D solar radiative transfer algorithm, Q. J. R. Meteorol. Soc., 125, 301–330, 1999.

Osborne, S., Baran, A., Johnson, B., Haywood, J., Hesse, E., and Newman, S.: Short-wave and long-wave radiative properties of Saharan dust aerosol, Q. J. Roy. Meteorol. Soc., 137, 1149–1167, 2011.

Osipov, S., Stenchikov, G., Brindley, H., and Banks, J.: Diurnal cycle of the dust instantaneous direct radiative forcing over the Arabian Peninsula, Atmos. Chem. Phys., 15, 9537-9553, doi:10.5194/acp-15-9537-2015, 2015.

Otto, S., de Reus, M., Trautmann, T., Thomas, A., Wendisch, M., and Borrmann, S.: Atmospheric radiative effects of an in situ measured Saharan dust plume and the role of large particles, Atmos. Chem. Phys., 7, 4887-4903, doi:10.5194/acp-7-4887-2007, 2007.

Papadimas, C. D., Hatzianastassiou, N., Matsoukas, C., Kanakidou, M., Mihalopoulos, N., and Vardavas, I.: The direct effect of aerosols on solar radiation over the broader Mediterranean basin, Atmos. Chem. Phys., 12, 7165-7185, doi:10.5194/acp-12-7165-2012, 2012.

Pérez, C., Nickovic, S., Pejanovic, G., Baldasano, J. M., and Özsoy, E.: Interactive dust-radiation modeling: A step to improve weather forecasts, J. Geophys. Res., 111, 1–17, 2006.

Pérez, C., Haustein, K., Janjic, Z., Jorba, O., Huneeus, N., Baldasano, J. M., Black, T., Basart, S., Nickovic, S., Miller, R. L., Perlwitz, J. P., Schulz, M., and Thomson, M.: Atmospheric dust modeling from meso to global scales with the online NMMB/BSC-Dust model – Part 1: Model description, annual simulations and evaluation, Atmos. Chem. Phys., 11, 13001-13027, doi:10.5194/acp-11-13001-2011, 2011.

Perlwitz, J., Tegen, I., and Miller, R.: Interactive soil dust aerosol model in the GISS GCM 1. Sensitivity of the soil dust cycle to radiative properties of soil dust aerosols, J. Geophys. Res., 106, 18167–18192, 2001.

Petzold, A., Rasp, K., Weinzierl, B., Esselborn, M., Hamburger, T., Dörnbrack, A., Kandler, K., Schütz, L., Knippertz, P., Fiebig, M., and Virkkula, A.: Saharan dust refractive index and optical properties from aircract-based observations during SAMUM 2006, Tellus B, 61 118–130, 2009.

Pey, J., Querol, X., Alastuey, A., Forastiere, F., and Stafoggia, M.: African dust outbreaks over the Mediterranean Basin during 2001–2011: PM10 concentrations, phenomenology and trends, and its relation with synoptic and mesoscale meteorology, Atmos. Chem. Phys., 13, 1395–1410, doi: 10.5194/acp-13-1395-2013, 2013.

Pincus, R., and Baker, M.: Precipitation, solar absorption and albedo susceptibility in marine boundary layer clouds, *Nature*, 372, 250– 252, 1994.

Atmos. Chem. Phys. Discuss., https://doi.org/10.5194/acp-2017-932
Manuscript under review for journal Atmos. Chem. Phys.
Discussion started: 10 November 2017

Atmospheric Chemistry and Physics
Discussions

Querol, X., Pey, J., Pandolfi, M., Alastuey, A., Cusack, M., Pérez, N., Moreno, T., Viana, N., Mihalopoulos, N., Kallos, G. and Kleanthous, S.: African dust contributions to mean ambient PM10 mass-levels across the Mediterranean basin, Atmos. Environ., 43, 4266–4277, doi:10.1016/j.atmosenv.2009.06.013, 2009.

Remer, L. A., Kaufman, Y. J., Tanré, D., Mattoo, S., Chu, D. A., Martins, J. V., Li, R. R., Ichoku, C., Levy, R. C., Kleidman, R. G., Eck, T. F., Vermote, E., and Holben, B. N.: The MODIS aerosol algorithm, products and validation, J. Atmos. Sci., 62, 947–973, doi:10.1175/JAS3385.1, 2005.

Rémy, S., Benedetti, A., Bozzo, A., Haiden, T., Jones, L., Razinger, M., Flemming, J., Engelen, R. J., Peuch, V. H., and Thepaut, J. N.: Feedbacks of dust and boundary layer meteorology during a dust storm in the eastern Mediterranean, Atmos. Chem. Phys., 15, 12909-12933, doi:10.5194/acp-15-12909-2015, 2015.

Rodríguez, S., Querol, X., Alastuey, A., Kallos, G., and Kakaliagou, O.: Saharan dust contributions to PM10 and TSP levels in Southern and Eastern Spain, Atmos. Environ., 35, 2433-2447, doi: 10.1016/S1352-2310(00)00496-9, 2001.

Roesch, A., Wild, M., Ohmura, A., Dutton, E. G., Long, C. N., and Zhang, T.: Assessment of BSRN radiation records for the computation of monthly means, Atmos. Meas. Tech., 4, 339-354, doi:10.5194/amt-4-339-2011, 2011.

Romano, S., Burlizzi, P., Perrone, M.R.: Experimental determination of short- and long-wave dust radiative effects in the Central Mediterranean and comparison with model results, Atmos. Res., 171, 5-20, 10.1016/j.atmosres.2015.11.019, 2016.

Santese, M., Perrone, M. R., Zakey, A. S., De Tomasi, F., and Giorgi, F.: Modeling of Saharan dust outbreaks over the Mediterranean by RegCM3: case studies, Atmos. Chem. Phys., 10, 133-156, doi:10.5194/acp-10-133-2010, 2010.

Sassen, K., DeMott, P. J., Prospero, J., and Poellot, M. R.: Saharan Dust Storms and Indirect Aerosol Effects on Clouds: CRYSTAL-FACE Results, Geophys. Res. Lett., 30, 12, 1633, doi:10.1029/2003GL017371, 2003.

Scarnato, B. V., China, S., Nielsen, K., and Mazzoleni, C.: Perturbations of the optical properties of mineral dust particles by mixing with black carbon: a numerical simulation study, Atmos. Chem. Phys., 15, 6913-6928, doi:10.5194/acp-15-6913-2015, 2015.

Schepanski, K., Tegen, I., Todd, M. C., Heinold, B., Bönisch, G., Laurent, B., and Macke, A.: Meteorological processes forcing Saharan dust emission inferred from MSG-SEVIRI observations of subdaily dust source activation and numerical models, J. Geophys. Res., 114, D10201, doi:10.1029/2008jd010325, 2009.

Seigel, R. B., van den Heever, S. C., and Saleeby, S. M.: Mineral dust indirect effects and cloud radiative feedbacks of a simulated idealized nocturnal squall line, Atmos. Chem. Phys., 13, 4467-4485, doi:10.5194/acp-13-4467-2013, 2013.

Sicard, M., Bertolín, S., Mallet, M., Dubuisson, P., and Comerón, A.: Estimation of mineral dust long-wave radiative forcing: sensitivity study to particle properties and application to real cases in the region of Barcelona, Atmos. Chem. Phys., 14, 9213–9231, doi:10.5194/acp-14-9213-2014, 2014a.

Sicard, M., Bertolín, S., Muñoz, C., Rodríguez, A., Rocadenbosch, F. and Comerón, A.: Separation of aerosol fine- and coarse-mode radiative properties: Effect on the mineral dust longwave, direct radiative forcing, Geophys. Res. Lett., 41, 6978–6985, doi:10.1002/2014GL060946, 2014.

Simmons, A. J. and Burridge, D. M.: An energy and angular momentum conserving vertical finite-difference scheme and hybrid vertical coordinates, Mon. Weather Rev., 109, 758–766, doi:10.1175/1520-0493(1981)1092.0.CO;2, 1981.

Singh, S. and Beegum, S.N.: Direct radiative effects of an unseasonal dust storm at a western Indo Gangetic Plain station Delhi in ultraviolet, shortwave, and longwave regions, Geophys. Res. Lett., 40, 2444-2449, doi: 10.1002/grl.50496, 2013.

Sokolik, I. N., Winker, D., Bergametti, G., et al.: Introduction to special section: outstanding problems in quantifying the radiative impacts of mineral dust, J. Geophys. Res., 106, 18 015–18 027, 2001.

Solmon, F., Mallet, M., Elguindi, N., Giorgi, F., Zakey, A., and Konare, A.: Dust aerosol impact on regional precipitation over Western Africa, mechanisms and sensitivity to absorption properties, Geophys. Res. Lett., 35, l24705, doi:10.1029/2008GL035900, 2008.

Solmon, F., Elguindi, N., and Mallet, M.: Radiative and climatic effects of dust over West Africa, as simulated by a regional climate model, Clim. Res., 2, 97–113, 2012.

Spyrou, C., Kallos, G., Mitsakou, C., Athanasiadis, P., Kalogeri, C., and Iacono, M. J.: Modeling the radiative effects of desert dust on weather and regional climate, Atmos. Chem. Phys., 13, 5489-5504, doi:10.5194/acp-13-5489-2013, 2013.

Stanelle, T., Vogel, B., Vogel, H., Bäumer, D., and Kottmeier, C.: Feedback between dust particles and atmospheric processes over West Africa during dust episodes in March 2006 and June 2007, Atmos. Chem. Phys., 10, 10771-10788, doi:10.5194/acp-10-10771-2010, 2010.

Tegen, I., Bierwirth, E., Heinold, B., Helmert, J., and Wendisch, M.,: Effect of measured surface albedo on modeled Saharan dust solar radiative forcing, J. Geophys. Res., 115, D24312, doi:10.1029/2009JD013764, 2010.

Theodosi, C., Markaki, Z., and Mihalopoulos, N.: Iron speciation, solubility and temporal variability in wet and dry deposition in the Eastern Mediterranean, Marine Chem., 120, 100–107, 2010.

Toledano, C., Cachorro, V. E., de Frutos, A. M., Sorribas, M., Prats, N., and de la Morena, B. A.: Inventory of African desert dust events over the southwestern Iberian Peninsula in 2000–2005 with an AERONET Cimel Sun photometer, J. Geophys. Res., 112, D21201, doi:10.1029/2006JD008307, 2007.

Torres, O., Bhartia P. K., Herman J. R., Ahmad Z., and Gleason J.: Derivation of aerosol properties from satellite measurements of backscattered ultraviolet radiation: Theoretical bases. J. Geophys. Res., 103, 17 009–17 110, 1998.

Torres, O., Tanskanen, A., Veihelman, B., Ahn, C., Braak, R., Bhartia, P. K., Veefkind, P., and Levelt, P.: Aerosols and Surface UV Products from OMI Observations: an overview, J. Geophys. Res., 112, D24S47, doi:10.1029/2007JD008809, 2007.

Twomey, S.: Pollution and the planetary albedo, *Atmos. Environ.*, 8, 1251– 1256, 1974.

Valenzuela, A., Olmo, F. J., Lyamani, H., Antón, M., Quirantes, A., and Alados-Arboledas, L.: Aerosol radiative forcing during African desert dust events (2005–2010) over Southeastern Spain, Atmos. Chem. Phys., 12, 10331-10351, doi:10.5194/acp-12-10331-2012, 2012.

Varga, G., Ùjvári, G., and Kovács, J.: Spatiotemporal patterns of Saharan dust outbreaks in the Mediterranean Basin, Aeolian Res., 15, 151–160, doi:10.1016/j.aeolia.2014.06.005, 2014.

Vinoj, V., Rasch, P. J., Wang, H., Yoon, J.-H., Ma, P.-L., Landu, K., and Singh, B.: Short-term modulation of Indian summer monsoon rainfall by West Asian dust, Nat. Geosci., 7, 308–313, doi:10.1038/NGEO2107, 2014.

Wang, H., Zhang, X. Y., Gong, S. L., Chen, Y., Shi, G.Y., and Li, W.: Radiative feedback of dust aerosols on the East Asian dust storms, J. Geophys. Res., 115, D23214, doi:23210.21029/22009JD013430, 2010.

Wang, H., Zhao, T. L., Zhang, X. Y., and Gong, S. L.: Dust direct radiative effects on the earth-atmosphere system over east Asia: Early spring cooling and late spring warming, Chinese Sci. Bull, 56, 1020–1030, doi:10.1007/s11434-011-4405-3, 2011.

Wang, H. and Niu, T.: Sensitivity studies of aerosol data assimilation and direct radiative feedbacks in modeling dust aerosols, Atmos. Environ., 64, 208–218, doi:10.1016/j.atmosenv.2012.09.066, 2013.

Wang, Z. L., Zhang, H., Jing, X. W., and Wei, X. D.: Effect of non-spherical dust aerosol on its direct radiative forcing, Atmos. Res., 120, 112–126, doi:10.1016/j.atmosres.2012.08.006, 2013.

Wang, H., Shi, G. Y., Zhu, J., Chen, B., Che, H., and Zhao, T. L.: Case study of longwave contribution to dust radiative effects over East Asia, Chin. Sci. Bull., 30, 3673–3681, doi:10.1007/s11434-013-5752-z, 2013.

Woodage, M.J., and Woodward, S.: U.K. HiGEM: Impacts of desert dust radiative forcing in a High-Resolution Atmospheric GCM, J. Clim., 27, 5907-5928, 2014.

Yang, E.-S., Gupta, P., and Sundar, A. C.: Net radiative effect of dust aerosols from satellite measurements over Sahara, Geophys. Res. Lett., 36, L18812, doi:10.1029/2009GL039801, 2009.

Yin, Y., Wurzler, S., Levin, Z., and Reisin, T. G.: Interactions of mineral dust particles and clouds: effects on precipitation and cloud optical properties, J. Geophys. Res., 107, 4724, doi:10.1029/2001JD001544, 2002.

Yin, Y. and Chen, L.: The effects of heating by transported dust layers on cloud and precipitation: a numerical study, Atmos. Chem. Phys., 7, 3497-3505, doi:10.5194/acp-7-3497-2007, 2007.

Yorks, J. E., McGill, M., Rodier, S., Vaughan, M., Hu, Y., and Hlavka, D.: Radiative effects of African dust and smoke observed from Clouds and the Earth's Radiant Energy System (CERES) and Cloud-Aerosol Lidar with Orthogonal Polarization (CALIOP) data, J. Geophys. Res., 114, D00H04, doi:10.1029/2009JD012000, 2009.

Yoshioka, M., Mahowald, N., Conley, A., Collins, W., Fillmore, D., and Coleman, D.: Impact of desert dust radiative forcing on Sahel precipitation: relative importance of dust compared to sea surface temperature variations, vegetation changes and greenhouse gas warming, J. Climate, 20, 1445–1467, 2007.

Zhang, D. F., Zakey, A. S., Gao, X. J., Giorgi, F., and Solmon, F.: Simulation of dust aerosol and its regional feedbacks over East Asia using a regional climate model, Atmos. Chem. Phys., 9, 1095-1110, doi:10.5194/acp-9-1095-2009, 2009.

Zhang, Z., Meyer, K., Platnick, S., Oreopoulos, L., Lee, D., and Yu, H.: A novel method for estimating shortwave direct radiative effect of above-cloud aerosols using CALIOP and MODIS data, Atmos. Meas. Tech., 7, 1777–1789, doi:10.5194/amt-7-1777-2014, 2014.

Zhang, Z., Meyer, K., Yu, H., Platnick, S., Colarco, P., Liu, Z., and Oreopoulos, L.: Shortwave direct radiative effects of above-cloud aerosols over global oceans derived from 8 years of CALIOP and MODIS observations, Atmos. Chem. Phys., 16, 2877-2900, doi:10.5194/acp-16-2877-2016, 2016.

Zhao, C., Liu, X., Leung, L. R., Johnson, B., McFarlane, S. A., Gustafson Jr., W. I., Fast, J. D., and Easter, R.: The spatial distribution of mineral dust and its shortwave radiative forcing over North Africa: modeling sensitivities to dust emissions and aerosol size treatments, Atmos. Chem. Phys., 10, 8821–8838, doi:10.5194/acp-10-8821-2010, 2010.

Zhao, C., Liu, X., Ruby Leung, L., and Hagos, S.: Radiative impact of mineral dust on monsoon precipitation variability over West Africa, Atmos. Chem. Phys., 11, 1879-1893, doi:10.5194/acp-11-1879-2011, 2011.

Zhu, A., Ramanathan, V., Li, F., and Kim, D.: Dust plumes over the Pacific, Indian, and Atlantic oceans: Climatology and radiative impact, J. Geophys. Res., 112, D16208,doi:10.1029/2007JD008427, 2007.

Atmos. Chem. Phys. Discuss., https://doi.org/10.5194/acp-2017-932
Manuscript under review for journal Atmos. Chem. Phys.
Discussion started: 10 November 2017

Table 1: List of the Mediterranean desert dust outbreaks which have been identified based on the satellite algorithm. In addition, the number of DD episodes (number of satellite grid cells at 1° x 1° spatial resolution where a DD episode has been identified), the regional intensity (in terms of AOD_{550nm}) calculated from the DD episodes as well as the dust affected parts of the Mediterranean domain are provided.

Case	Date	DD episodes	Intensity	Affected parts of the Mediterranean domain
1	31 July 2001	85	0.74	Western
2	8 May 2002	71	1.60	Central
3	4 April 2003	53	1.42	Eastern
4	16 July 2003	83	0.98	Western and Central
5	22 February 2004	46	2.18	Central and Eastern
6	26 March 2004	66	1.45	Central and Eastern
7	27 January 2005	37	1.36	Central and Eastern
8	2 March 2005	45	2.96	Central and Eastern
9	28 July 2005	30	1.08	Western and Central
10	24 February 2006	45	2.92	Eastern
11	19 March 2006	39	1.37	Eastern
12	24 February 2007	42	2.29	Central and Eastern
13	21 April 2007	42	1.65	Central
14	29 May 2007	47	1.40	Eastern
15	10 April 2008	42	1.58	Central
16	19 May 2008	66	1.45	Central
17	23 January 2009	36	2.65	Eastern
18	6 March 2009	41	1.41	Eastern
19	27 March 2010	39	1.43	Central
20	2 August 2012	35	1.20	Western

Atmos. Chem. Phys. Discuss., https://doi.org/10.5194/acp-2017-932
Manuscript under review for journal Atmos. Chem. Phys.
Discussion started: 10 November 2017

Atmospheric Chemistry and Physics Discussions

Table 2: Mean and standard deviation of clear-sky DRE_{TOA}, DRE_{SURF}, $DRE_{NETSURF}$ and DRE_{ATM} values, over the simulation period (84 hours), calculated in the NSD, SDD and MSD domains for the SW, LW and NET radiation. Blue and red background colors indicate negative (cooling effect) and positive (warming effect) DREs, respectively.

		DRE_{TOA}	**DRE_{SURF}**	**$DRE_{NETSURF}$**	**DRE_{ATM}**
NSD	**SW**	-5.1±5.9	-24±21.1	-17.1±15	12±12.6
	LW	1.7±1.3	3.3±0.7	5.5±1.8	-3.8±0.7
	NET	-3.4±5.6	-20.7±21.6	-11.6±13.4	8.2±12.2
SDD	**SW**	-3.4±6.1	-23.7±21.3	-15.9±14.3	12.5±13.4
	LW	1.8±1.5	3.6±0.8	6±2.2	-4.2±0.8
	NET	-1.6±6.1	-20.1±21.9	-9.9±12.4	8.3±13
MSD	**SW**	-9.7±8.8	-25.8±23.2	-20.4±18.5	10.6±11.2
	LW	1.5±0.8	3.1±0.8	4.8±1.2	-3.3±0.6
	NET	-8.2±8.2	-22.7±23.6	-15.6±17.5	7.3±11

Atmos. Chem. Phys. Discuss., https://doi.org/10.5194/acp-2017-932
Manuscript under review for journal Atmos. Chem. Phys.
Discussion started: 10 November 2017

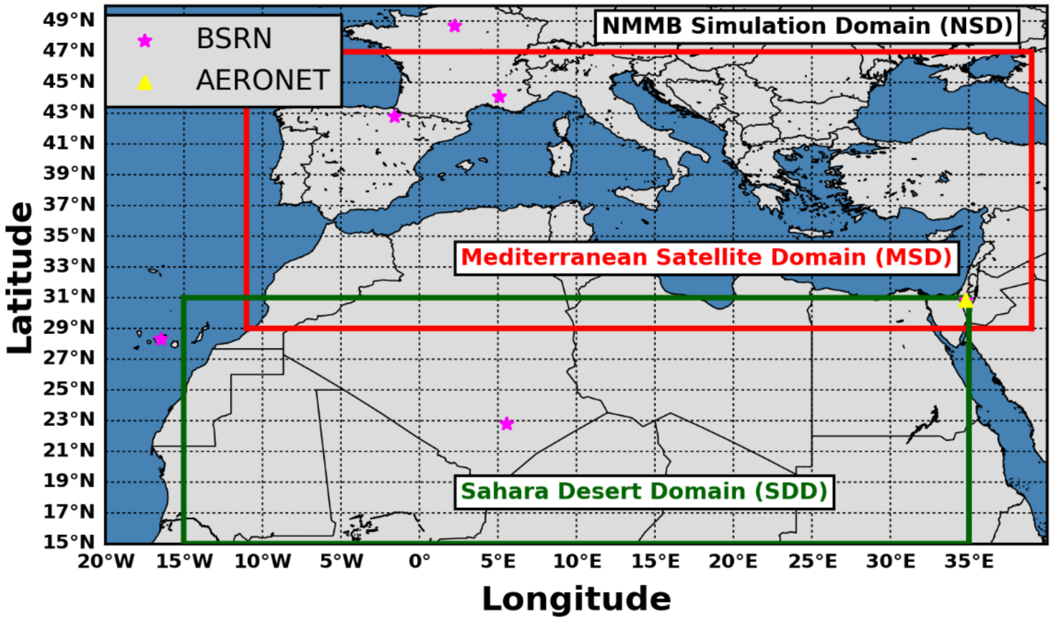

Figure 1: Geographical limits of the: (i) NMMB Simulation Domain (*NSD*, outer domain), (ii) Mediterranean Satellite Domain (*MSD*, red rectangle) and (iii) Sahara Desert Domain (*SDD*, green rectangle). With the magenta star symbols are depicted the locations of the BSRN stations and with the yellow triangle is denoted the location of the AERONET Sede Boker station.

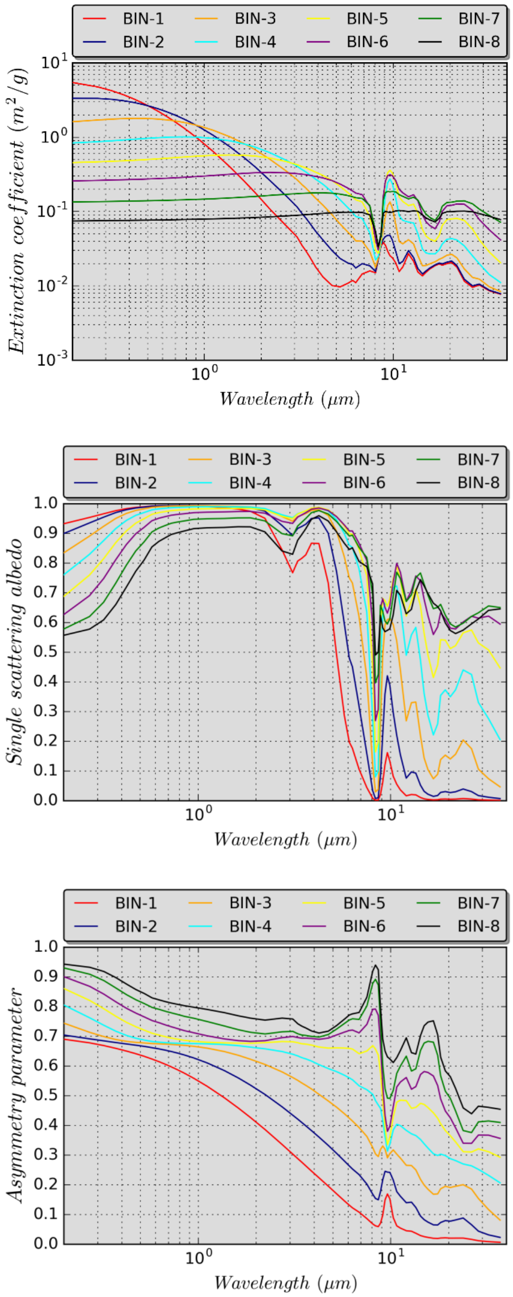

(i) (ii) (iii)

Figure 2: Spectral variation of the GOCART: (i) extinction coefficient (in m^2/g), (ii) single scattering albedo and (iii) asymmetry parameter, for each one of the 8 dust bins which are considered in the dust module.

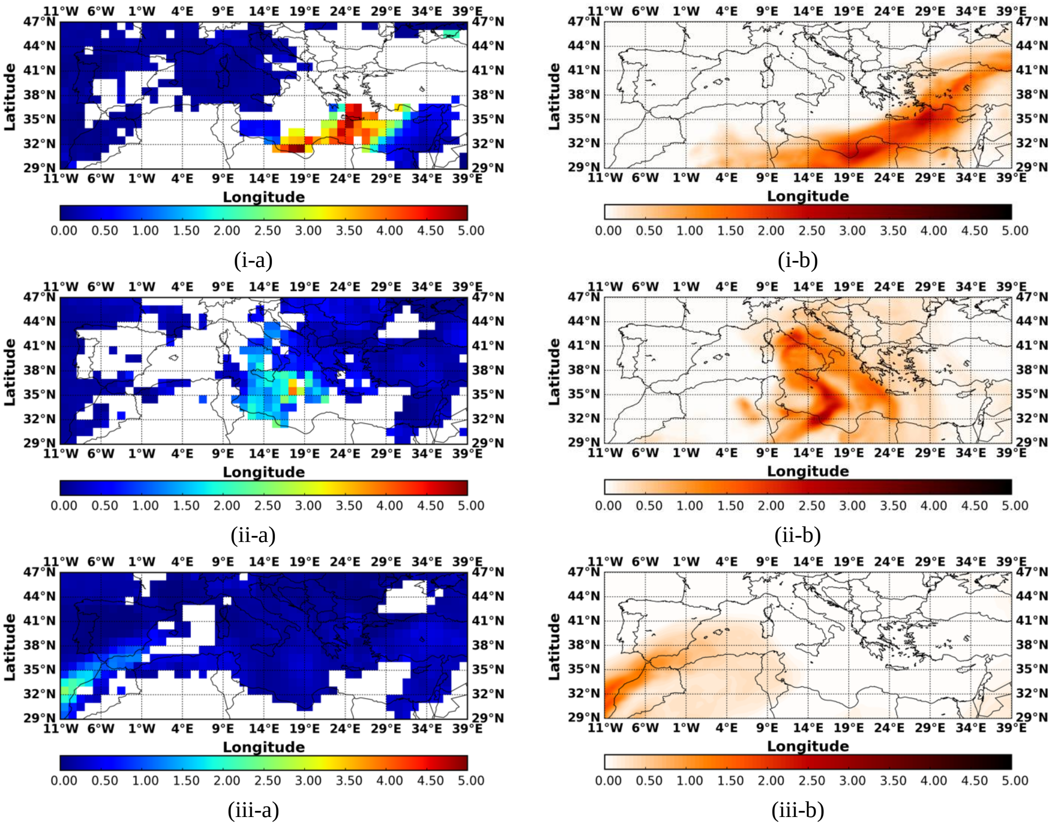

Figure 3: Geographical distributions of: (a) the daily averaged MODIS-Terra AOD at 550nm and (b) the simulated dust AOD at 550nm at 12:00 UTC for the Mediterranean desert dust outbreaks that took place on: (i) 2nd March 2005, (ii) 19th May 2008 and (iii) 2nd August 2012.

Atmos. Chem. Phys. Discuss., https://doi.org/10.5194/acp-2017-932
Manuscript under review for journal Atmos. Chem. Phys.
Discussion started: 10 November 2017

Atmospheric Chemistry and Physics
Open Access
EGU
Discussions

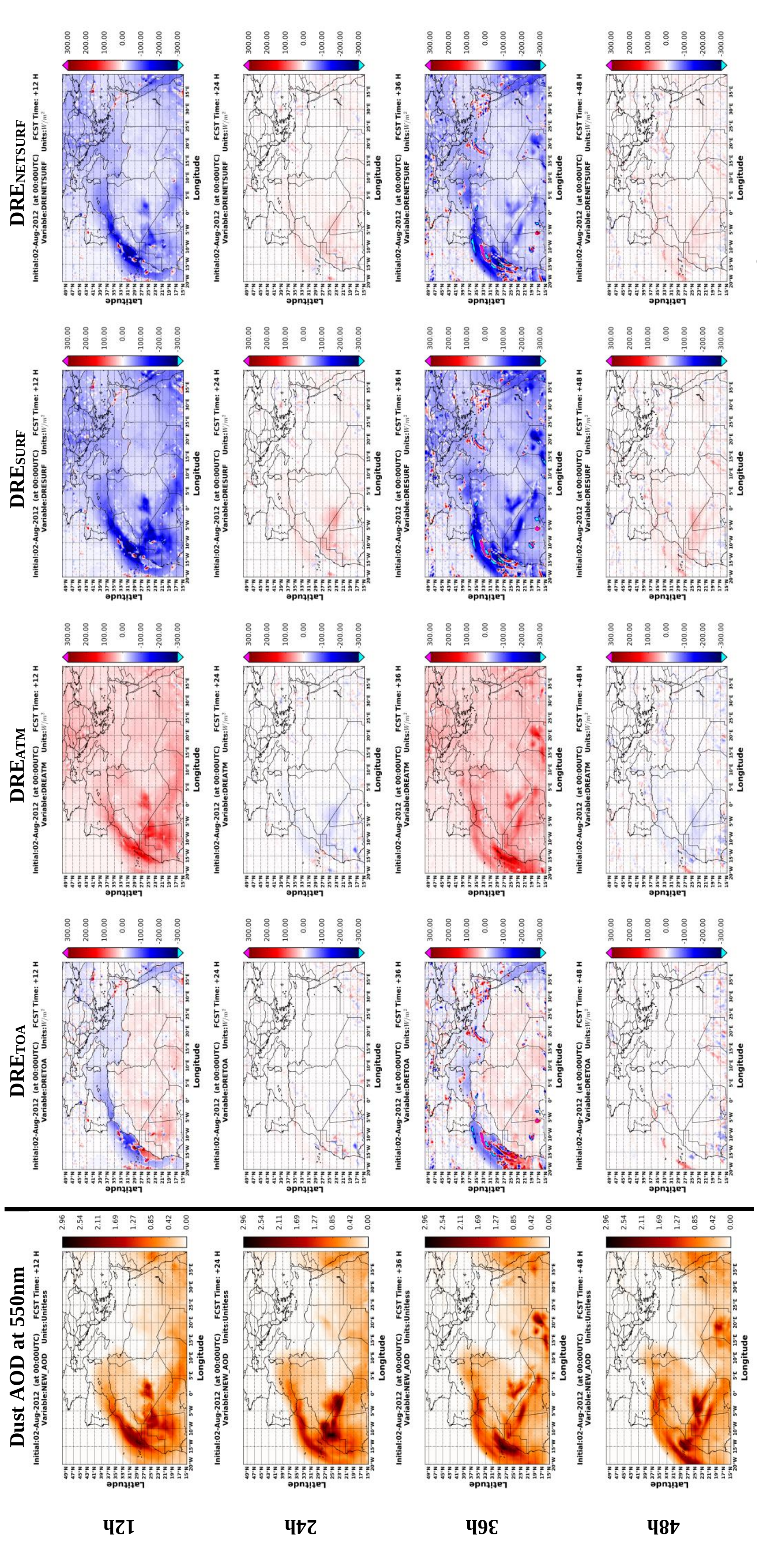

Figure 4: Spatial patterns of the simulated dust AOD_{550nm} and the instantaneous DRE_{TOA}, DRE_{ATM}, DRE_{SURF} and $DRE_{NETSURF}$ values, expressed in Wm^{-2}, at 12, 24, 36 and 48 hours after the initialization of NMMB-MONARCH model at 00 UTC on 2nd August 2012.

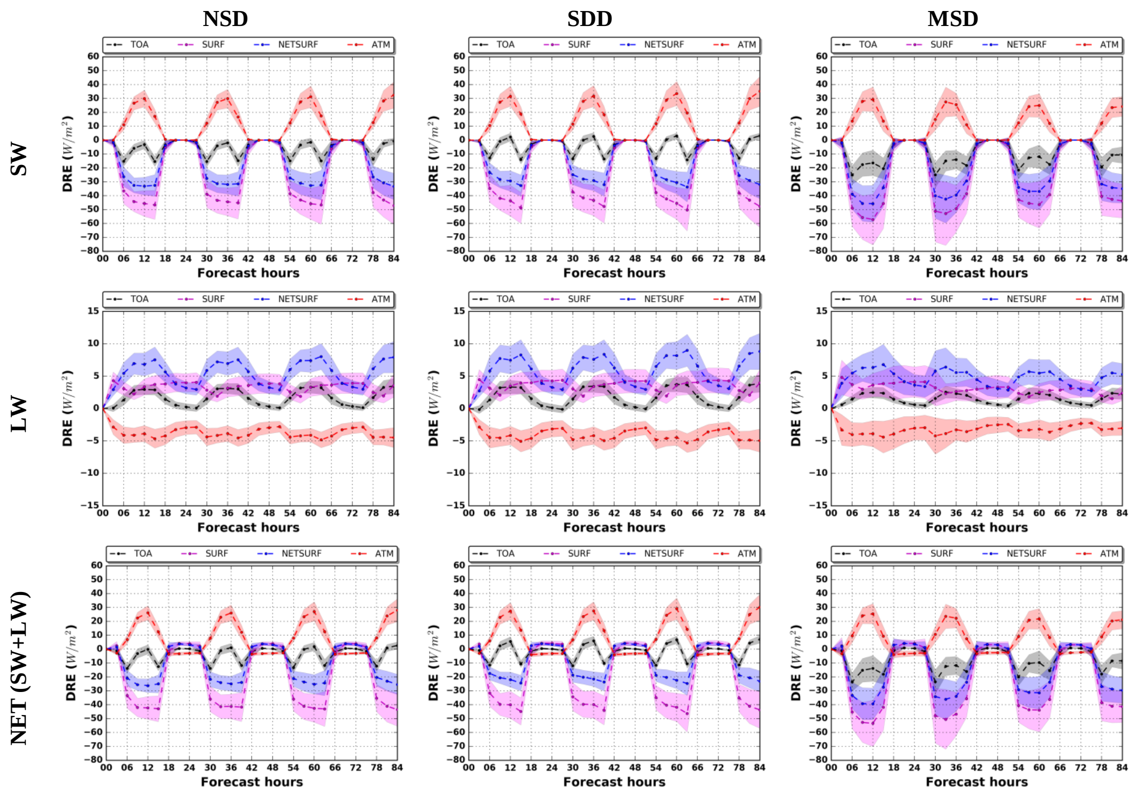

Figure 5: Regional clear-sky SW (upper row), LW (middle row) and NET (SW+LW) (bottom row) DREs at TOA (black), SURF (purple), NETSURF (blue) and ATM (red) averaged over the NSD (left column), SDD (central column) and MSD (right column) domains. The calculated DREs correspond to the mean values calculated by the 20 simulated Mediterranean desert dust outbreaks and the shaded areas represent the associated standard deviation.

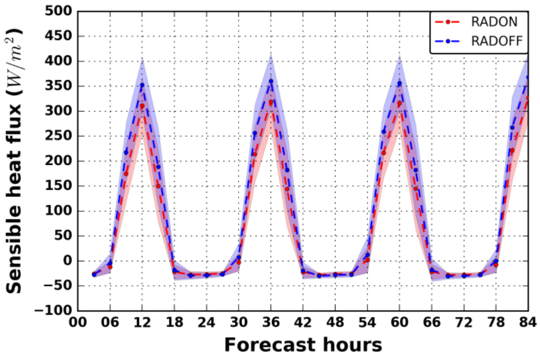

(i)

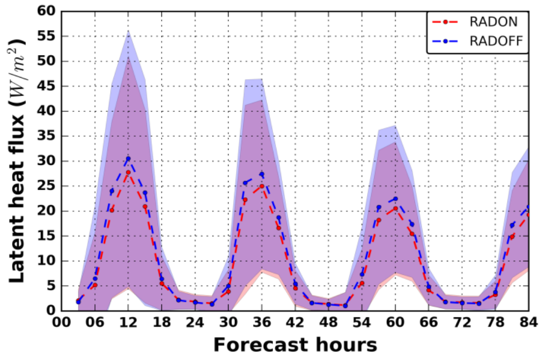

(ii)

Figure 6: Regional averaged values, over land areas of the simulation domain affected by dust loads and under clear-sky conditions, of the: (i) sensible and (ii) latent heat fluxes, expressed in Wm^{-2}, based on the RADON (red) and the RADOFF (blue) configuration of the NMMB-MONARCH model. The dashed lines correspond to the mean values calculated by the 20 simulated Mediterranean desert dust outbreaks and the shaded areas represent the associated standard deviation.

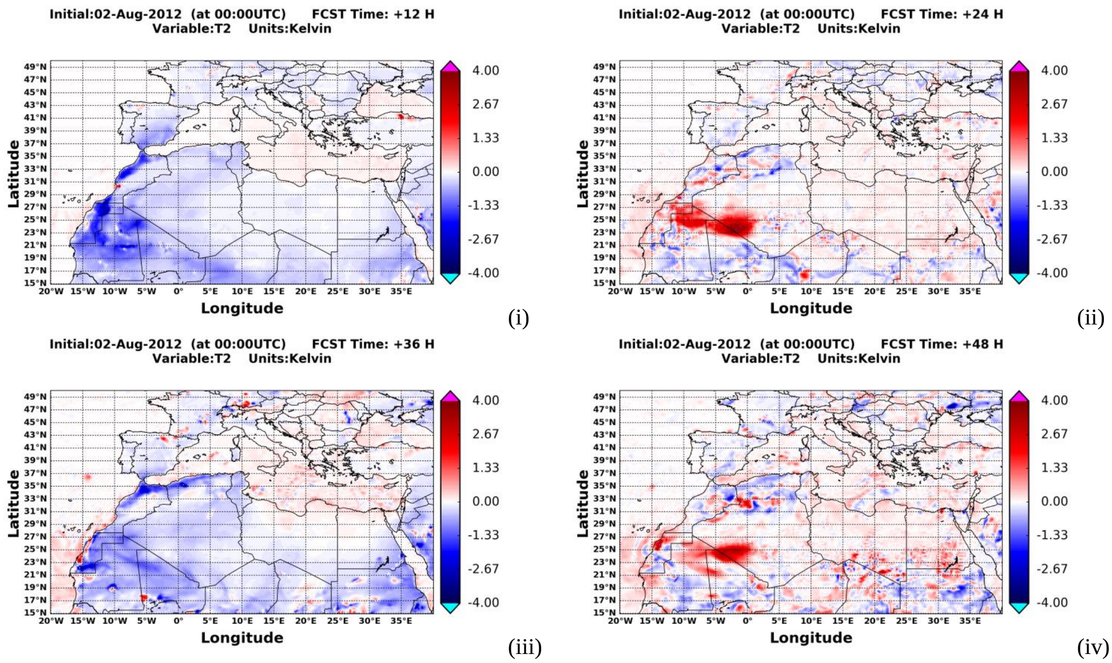

Figure 7: Spatial patterns of temperature differences at 2 meters, between the RADON and RADOFF configuration of the NMMB-MONARCH model, for the: (i) 12, (ii) 24, (iii) 36 and (iv) 48 hours forecast of the 00 UTC cycle on 2nd August 2012.

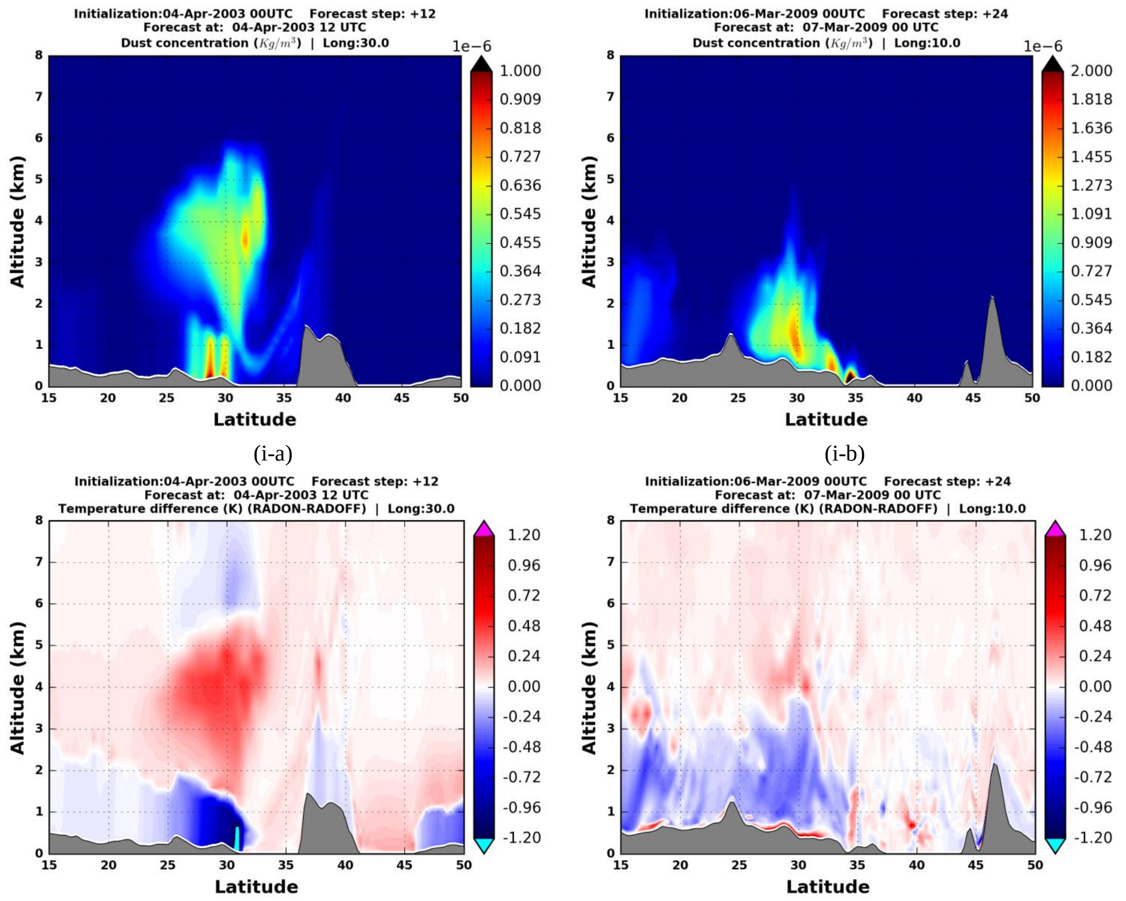

(ii-a) (ii-b)

Figure 8: Altitude-latitude cross-sections (up to 8 km m.s.l.) simulated by the NMMB-MONARCH model of the: (i) dust concentration (in kg m^{-3}) and (ii) RADON-RADOFF temperature anomalies (in K) on: (a) 4 April 2003 at 12 UTC along the meridional 30° E and (b) 7 March 2009 00 UTC along the meridional 10° E.

Atmos. Chem. Phys. Discuss., https://doi.org/10.5194/acp-2017-932
Manuscript under review for journal Atmos. Chem. Phys.
Discussion started: 10 November 2017

Atmospheric Chemistry and Physics Discussions
Open Access
EGU

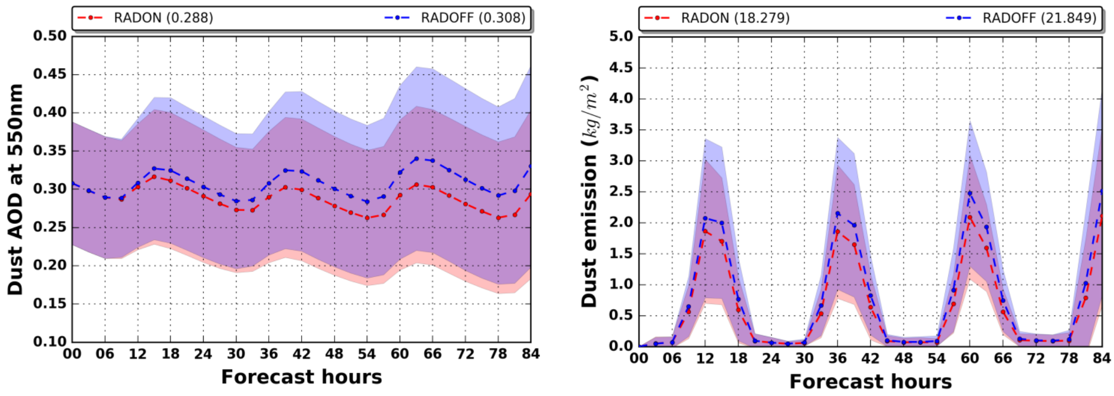

(i) (ii)

Figure 9: (i) Regional dust AOD at 550nm averaged over the simulation domain (NSD) and (ii) Regional dust emission (in kg m^{-2}) aggregated over the simulation domain (NSD). Blue and red curves correspond to the mean values, calculated from the 20 desert dust outbreaks, for the RADOFF and RADON simulations, respectively, and the shaded areas represent the associated standard deviation.

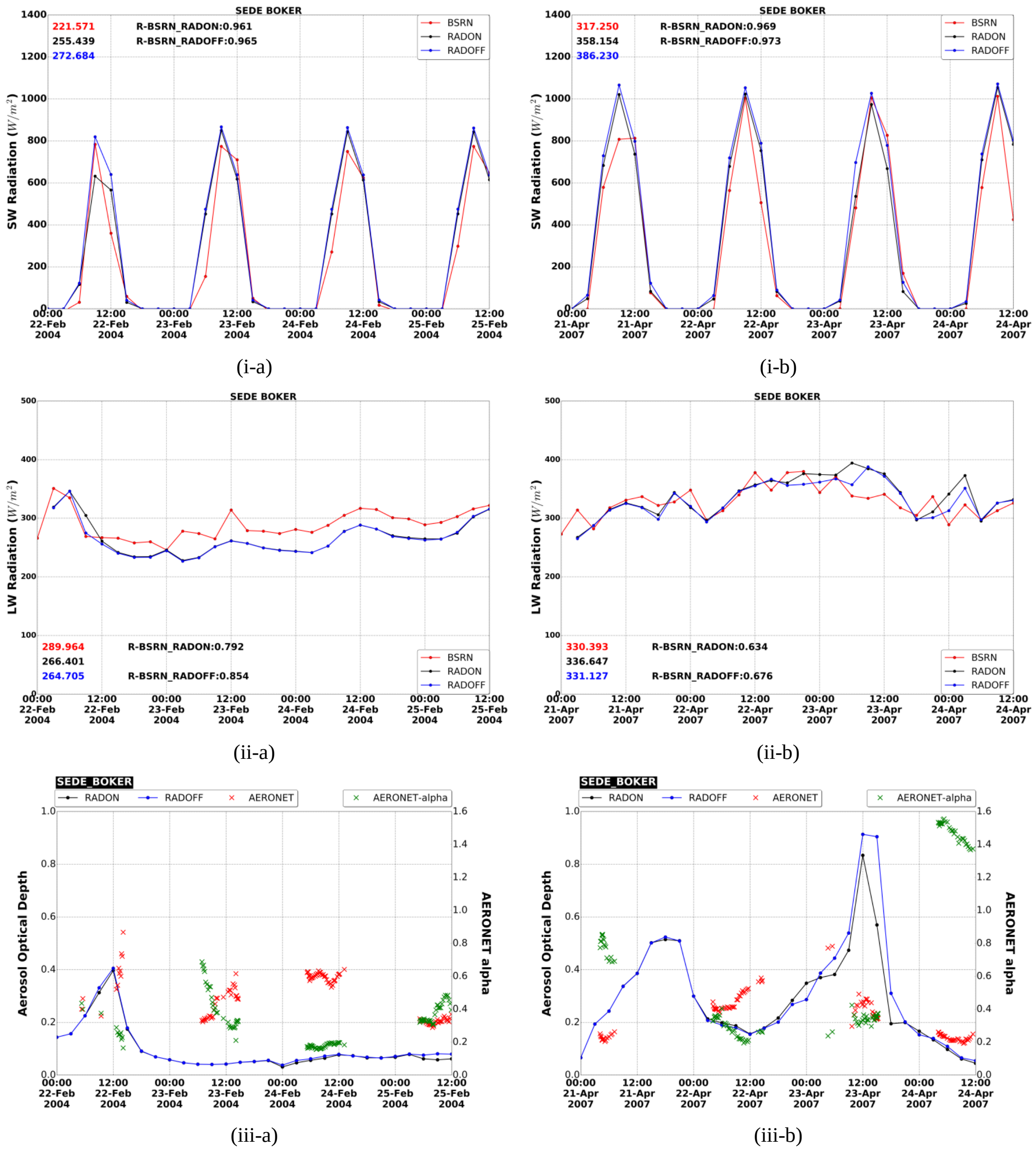

Figure 10: Timeseries of the downwelling: (i) SW and (ii) LW radiation measured at Sede Boker (red line) and simulated based on the RADON (black line) and RADOFF (blue line) configuration of the NMMB-MONARCH model during the periods: (a) 22 Feb. 2004 00UTC – 25 Feb. 2004 12UTC and (b) 21 Apr. 2007 00UTC – 24 Apr. 2007 12UTC. The mean ground and modelled values along with the computed correlation coefficients (R) between RADON-BSRN and RADOFF-BSRN, both calculated over the simulation periods, are also provided. (iii) Timeseries of the simulated dust AOD at 550 nm for the RADON (black line) and RADOFF (blue line) configuration of the NMMB-MONARCH model. Moreover, the AERONET total AOD at 500 nm (red) and AERONET alpha (green) values are provided.

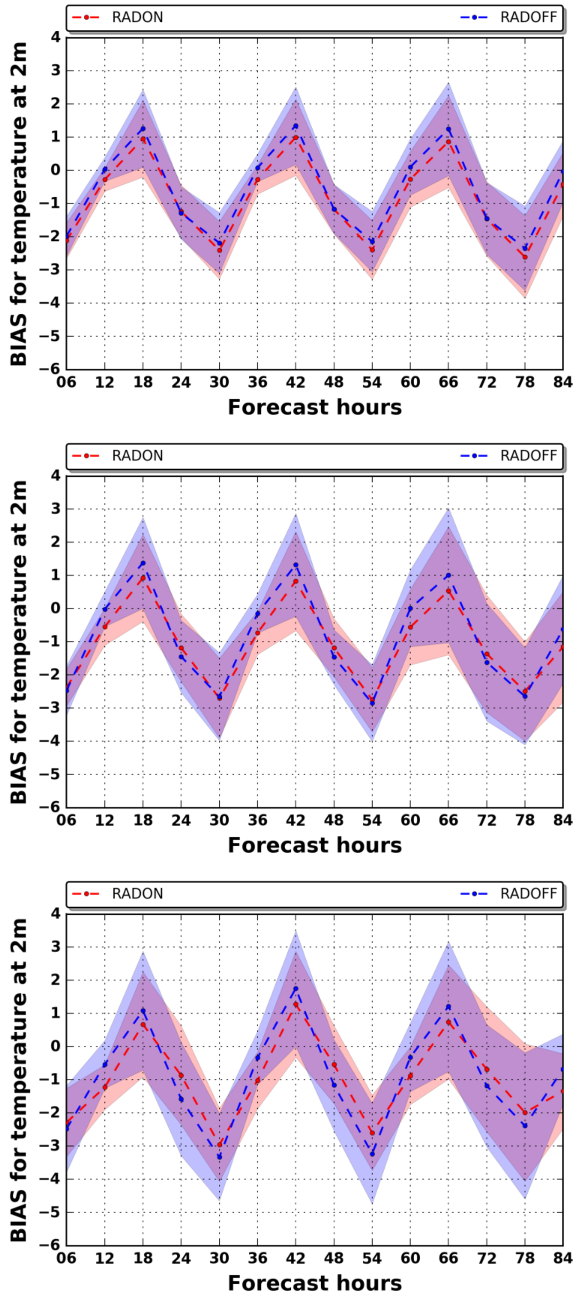

(i)

(ii)

(iii)

Figure 11: Regional biases of temperature at 2 meters between NMMB-MONARCH and FNL, at 1°x1° degrees spatial resolution, calculated over land grid points of the simulation domain (NSD) in which dust AOD at 550 nm is higher/equal than: (i) 0.1, (ii) 0.5 and (iii) 1.0.

Atmos. Chem. Phys. Discuss., https://doi.org/10.5194/acp-2017-932
Manuscript under review for journal Atmos. Chem. Phys.
Discussion started: 10 November 2017

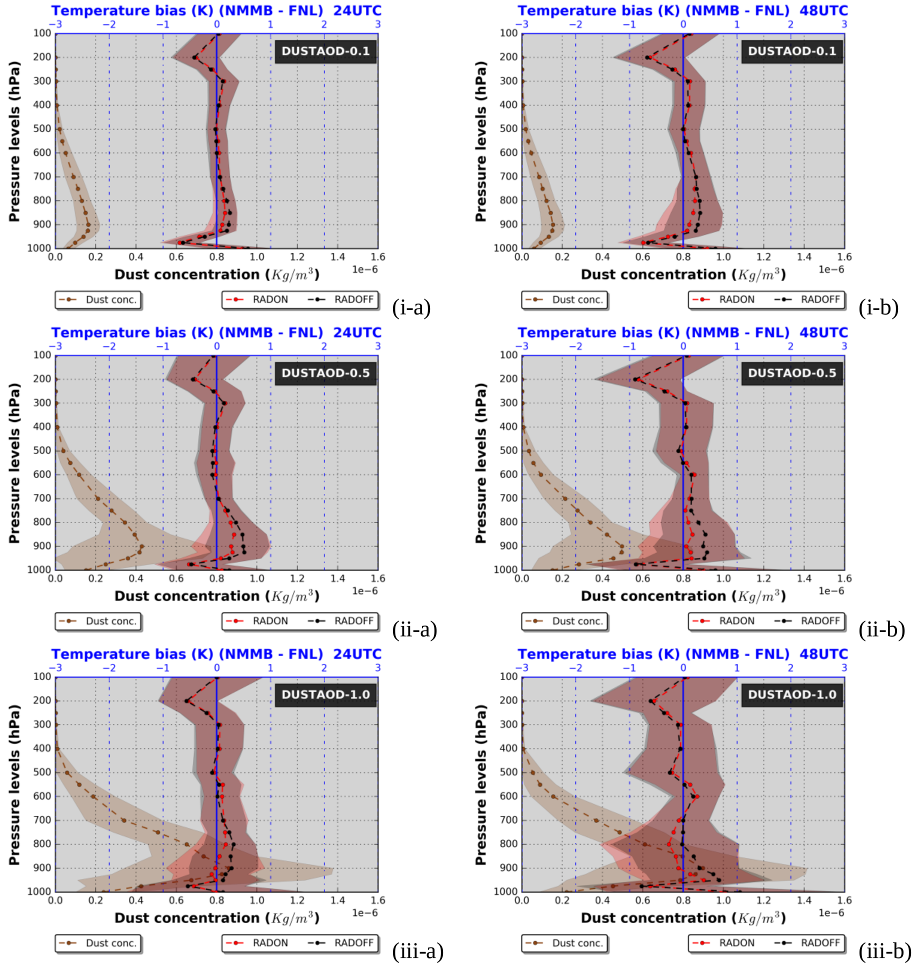

Figure 12: Vertical profiles of the regional temperature RADON-FNL (red curve) and RADOFF-FNL (black curve) biases calculated over grid points (1° x 1° degrees spatial resolution) where the dust AOD at 550 nm is higher/equal than: (i) 0.1, (ii) 0.5 and (iii) 1.0. In addition, the vertical profiles of the simulated dust concentration (in x10^{-6} kg m^{-3}) are provided (brown curve). Each profile corresponds to the mean value calculated from the 20 desert dust outbreaks which are considered while the shaded areas correspond to the associated standard deviations. The obtained results are valid: (a) 24 and (b) 48 hours after the initialization of the forecast period.